Experimental study of dissolution rates of hedenbergitic clinopyroxene at high temperatures: dissolution in water from 25°C to 374°C

Ronghua Zhang, Xuetong Zhang, Bernard Guy, Shumin Hu, Dominique de Ligny, Jacques Moutte

Eur. J. Mineral.
2013, **25**, 353–372
Published online April 2013

Experimental study of dissolution rates of hedenbergitic clinopyroxene at high temperatures: dissolution in water from 25 °C to 374 °C

RONGHUA ZHANG[1,*], XUETONG ZHANG[1], BERNARD GUY[2], SHUMIN HU[1], DOMINIQUE DE LIGNY[3] and JACQUES MOUTTE[2]

[1] Laboratory of Geochemical Kinetics, MLR Key Laboratory of Metallogeny and Mineral Assessment, Institute of Mineral Resources, Chinese Academy of Geological Sciences, 100037 Beijing, China
*Corresponding author, e-mail: zrhhsm@pku.edu.cn
[2] Ecole nationale supérieure des mines de Saint-Etienne, Centre SPIN (Sciences des Processus Industriels et Naturels), Unit of Geochemistry, Saint-Etienne, France
[3] Laboratoire de physico-chimie des matériaux luminescents, Université Lyon 1, Villeurbanne, France

Abstract: Steady-state pyroxene dissolution rates in aqueous solutions have been measured at temperatures from 25 to 374 °C at a pressure of 23 MPa and at neutral pH. The pyroxene is hedenbergitic clinopyroxene, of composition $Na_{0.04}Ca_{0.95}Mg_{0.3}Fe^{2+}_{0.64}Fe^{3+}_{0.06}Al_{0.04}Si_{1.97}O_6$. All experiments were performed at conditions far from equilibrium in Ti-alloy mixed-flow reactors. In most runs, the reactive solutions were undersaturated with respect to pyroxene and secondary minerals were rarely found at the reacted surface. The dissolution is non-stoichiometric in most cases, while the different chemical elements of the pyroxene are released at different rates. Stoichiometric steady-state dissolution was obtained in neutral solution at 100 °C.

The release rates of the different elements vary with temperature and solution chemistry. The dissolution rates (r_{Si}) in neutral pH conditions increase with temperature from 25 to 300 °C, reach a maximum at 300 °C, and then decrease with continued temperature increase. At a given temperature, the rates decrease significantly with increasing pH of the reactive fluid and are also affected by the activities of Ca, Mg, Fe in the solution. At neutral pH, the dependence of the pyroxene dissolution rates on activities of Ca, Mg, Fe and H^+ in the fluid can be expressed by the relation:

$$\log r_+(T, a_i) = \log (A - E_a/(2.303\,RT) + \alpha \log (a_{H^+})^{Zi}/a_{M_i{}^{Zi+}})$$

where r_+ is the far-from-equilibrium dissolution rate, R the gas constant, T the absolute temperature, Z_i valence of metal M_i and a_i represents the activity of the subscript aqueous species. E_a equals 22.667 kJ/mole/K and $A = 2.011 \times 10^{-7}$ mole/cm^2/s; α is the empirical reaction rate order, which can be derived from the experimental results.

At temperatures below 300 °C, the exchange reactions $2H^+ \leftrightarrow M_i{}^{2+}$, where $M_i{}^{2+}$ refers to divalent cations Mg^{2+}, Fe^{2+} or Ca^{2+}, dominate in the dissolution. The following evolution of the dissolution with temperature is proposed: at 300 °C, the tetrahedral Si–O bonds break after the $M_i{}^{2+}$–O bonds in adjacent octahedral positions have been removed by proton exchange reaction, whereas, above 300 °C, the breaking of the octahedral $M_i{}^{2+}$–O bonds occurs after adjacent tetrahedral Si–O bonds have been broken.

Key-words: dissolution, kinetics, high temperature, hedenbergite, clinopyroxene, rate, critical state, mineral surface.

1. Introduction

The present study of pyroxene dissolution rates at high temperatures up to 374 °C is motivated by two important reasons.

The first reason is that pyroxene is a typical multi-oxide silicate mineral. The dissolution of a multi-oxide mineral in water requires the breaking of more than one type of metal–oxygen bond. When such minerals dissolve, the nature of the metal–oxygen bond may affect the rate at which the metal is released to the aqueous solution. It appears necessary to improve our understanding of the mechanism of dissolution of pyroxene or pyroxenoid minerals as a function of temperature above 300 °C. Moreover, the variation of the release rates of the different metals with temperature is not easy to interpret, particularly at high temperatures. Some experiments of mineral dissolution are performed at temperatures higher than 300 °C; water then is close to the critical state, its properties strongly vary and this affects the reaction behaviour (Levelt Sengers, 2000).

The second reason is that reactions between pyroxene and aqueous solutions at high temperatures play an

0935-1221/13/0025-2268 $ 9.00
DOI: 10.1127/0935-1221/2013/0025-2268

important role in a large number of hydrothermal and metamorphic processes. Pyroxene is an important mineral in many igneous and metamorphic rocks and is common in many types of ore deposits. The dissolution rates of pyroxene at high temperatures govern the water-rock interactions at depth, for instance at mid-ocean ridges or in gabbros of the oceanic crust.

The desire to quantify these processes has led to a series of high-temperatures dissolution experiments on silicate minerals, but only few studies have been carried out on multi-oxide silicates above 300 °C (Lasaga, 1981; Aagaard & Helgeson, 1982; Murphy & Helgeson, 1987, 1989; Alekseyev *et al.,* 1993, 1997; Oelkers, 2001). Concerning the dissolution mechanism of pyroxene, several studies have reported dissolution rates above 100 °C (*e.g.*, Knauss *et al.,* 1993; Oelkers & Schott, 2001; Dixit & Carroll, 2007).

The present experiments on the dissolution of pyroxene in aqueous solutions at neutral pH and temperatures up to 374 °C will provide new information on the controlling factors of the high-temperature dissolution of a multi-oxide mineral. Another objective of the present work is to compare the results bearing on Fe-rich clinopyroxene with those obtained for more Mg-rich clinopyroxene. It happens that, at temperatures below 300 °C, Fe-O bonds do break faster than Si-O bonds, as do Mg-O bonds (Guy, 2003; Nourtier-Mazauric *et al.,* 2005).

2. Research background and problems

2.1. Within a multi-oxide silicate structure, each type of metal-oxygen bond breaks at a distinct rate

There are relatively large differences between the rates at which the various metal-oxygen bonds of a multi-oxide silicate mineral break, when the mineral dissolves in an aqueous solution. As a result, the dissolution is often not stoichiometric, and the ratios between the various dissolving metal species differ from their stoichiometric proportions in the mineral (Hellmann *et al.,* 1989; Welch & Ullman, 1993, 1996; Stillings & Brantley, 1995; Stillings *et al.,* 1995, 1996; Chen & Brantley, 1998; Oelkers & Schott, 1999, 2001; Oelkers, 2001; Zhang *et al.,* 2000, 2002; Dixit & Carroll, 2007). As pyroxene dissolves in water, a given cation M_i (M_i = Si, Al, Na, Ca, Mg,...) is removed from the surface layers and released to the solution. If the rates at which the various metal–oxygen bonds break are variable, a so-called ''leached layer'', relatively depleted in some metals, enriched in other, will form upon the mineral surface.

For multi-oxide silicate minerals such as pyroxene and feldspar, univalent and divalent cations are released first, followed by aluminium, then by silica. Previous studies on the dissolution of silicate minerals at temperatures below 300 °C indicate the development of a silica-enriched layer on the mineral surface (for forsterite, Pokrovsky & Schott, 2000; Oelkers, 2001; for diopside, Schott *et al.,* 1981; Schott & Berner, 1985; Petit *et al.,* 1987; Peck *et al.,* 1988; Dixit & Carroll, 2007; for hornblende, Frogner & Schweda, 1998; for smectite, Hofmann *et al.,* 2004; Metz *et al.,* 2005; for actinolite, Zhang *et al.,* 2007a and b; for albite, Hellmann *et al.,* 1989; Oelkers *et al.,* 1994; Zhang *et al.,* 2002; for talc, Saldi *et al.,* 2007; for muscovite, Oelkers *et al.,* 2008). These studies indicate that dissolution proceeds by the sequential removal of metals from the mineral structure; the order of the removal of each metal is dictated by the relative rates of breaking of each metal–oxygen bond.

A variety of evidence suggests that octahedral M_i–O bonds break more rapidly than tetrahedral Si–O bonds. In the pyroxene structure (*e.g.* enstatite), which consists of chains of silica tetrahedra linked together by magnesium in octahedral position, the Mg–O bonds apparently break more rapidly than the Si–O bonds (Oelkers & Schott, 2001).

The dissolution rate of a multi-oxide silicate mineral may be calculated independently from the release of each of the different major elements that occupy tetrahedral and octahedral sites. When these calculations yield the same dissolution rate for each metal, the dissolution can be considered as stoichiometric. Non-stoichiometric dissolution may be explained by the following mechanisms: (1) precipitation of a new phase (*e.g.* a secondary mineral) at the surface, and (2) dissolution of the secondary mineral; (3) preferential dissolution of one or more components (elements) and formation of a leached layer enriched in the other components; (4) chemical zonation of the dissolved mineral or presence of non-homogeneous defects or impurities (Petrovic, 1976; Schott & Petit, 1987; Brantley & Chen, 1995; Bauer & Berger, 1998; Sutheimer *et al.,* 1999; Brandt *et al.,* 2003; Kohler *et al.,* 2003; Sato *et al.,* 2003; Hofmann *et al.,* 2004; Metz *et al.,* 2005; Zhu *et al.,* 2006, 2010; Saldi *et al.,* 2007; Oelkers *et al.,* 2008; Zhu and Lu, 2009). By definition, steady-state kinetics is obtained in flow-through reactors when dissolution rates are time independent, *i.e.* when the concentrations of metals in the effluent solution do not change with elapsed time.

2.2. Far-from-equilibrium dissolution rate

Within the context of Transition State Theory, surface-reaction-controlled dissolution rates can be considered to be

$$r = r_+(1 - \exp(\Delta G_r/\sigma RT)) \quad (1)$$

where ΔG_r is the free energy change for the overall dissolution reaction (Aagaard & Helgeson, 1977, 1982; Lasaga, 1981; Helgeson *et al.,* 1984; Oelkers, 2001), and where σ is Temkin's average stoichiometric number, *i.e.* the ratio of the rate of destruction of the activated or precursor complex to the overall rate, where r and r_+ designate the overall and forward dissolution rate, respectively; R designates the gas constant, and T represents the absolute temperature.

The dissolution rates in the present study were measured at far-from-equilibrium conditions, *i.e.* with $\Delta G_r << \sigma RT$;

they thus correspond to factor r_+ of relation (1). They can be used to assess the effect of aqueous solution composition on forward dissolution rates, independently from the ΔG_r effects.

Within the framework of the Transition State Theory, r_+ is proportional to the concentration of the rate controlling ''precursor complex'', in accord with Wieland *et al.* (1988):

$$r_+ = k_+ s[P^\bullet]. \quad (2)$$

where k_+ refers to a rate constant, s stands for the mineral/fluid interfacial surface area and $[P^\bullet]$ designates the concentration of the precursor complex, which itself is proportional to the concentration of the activated complex. The variation of r_+ with aqueous composition, therefore, can be deduced from mass action law applied to the reaction forming the precursor complex from the original mineral (*cf.* Oelkers, 2001).

The identity of the rate-controlling precursor complex P•, and its change with the aqueous solution composition, depend on the dissolution mechanism considered. For multi-oxide minerals, the dissolution mechanisms are considered to consist of sequential breaking of distinct metal oxygen bonds via metal-proton exchange reactions (Gautier *et al.,* 1994; Oelkers *et al.,* 1994; Oelkers & Schott, 1999, 2001; Oelkers, 2001; Harouiya & Oelkers, 2004; Carroll & Knauss, 2005; Chaïrat *et al.,* 2007; Dixit & Carroll, 2007; Saldi *et al.,* 2007).

As emphasized above, the precursor complex for multi-oxide mineral dissolution consists of the partially liberated metals near the mineral surface. Assuming the 1 to i-th metal needs to be removed to create the rate-controlling precursor complex, and all of the metal-proton exchange reactions are thermodynamically independent, the mole fraction of the precursor complex (X_p) is given by Gautier *et al.* (1994) and Oelkers, (2001) as

$$X_p = \prod_{i=1}^{\hat{i}} \left[K_i \left(\frac{a_{H^+}^{Z_i}}{a_{M_i^{Z_i+}}} \right)^{n_i} \Big/ \left(1 + K_i \left(\frac{a_{H^+}^{Z_i}}{a_{M_i^{z_i+}}} \right)^{n_i} \right) \right] \quad (3)$$

where a_i refers to the activity of the subscript aqueous species i, K_i is the equilibrium constant of the proton/metal M_i exchange reaction, Z_i is the valence of metal M_i; n_i denotes a stoichiometric coefficient, which equals the number of partially detached Si tetrahedral structures formed by the removal of each M_i.

2.3. Controlling factor on dissolution stoichiometry

If a multi-oxide silicate dissolution process is nearly stoichiometric, one can determine its rate law. Usually, in a first approximation (see Discussion section), the dissolution rates of multi-oxide silicate minerals at far from equilibrium conditions can be described using (Oelkers, 2001; Saldi *et al.,* 2007)

$$-r = k \left[(a_{H^+})^{Zi} / a_{M_i^{Z_i+}} \right]^{\alpha} \quad (4)$$

where k is the rate constant and α is the order with respect to the hydrogen ion activity *vs*. the activity of dissolved species M_i^{Zi+}, such as Ca, Mg, Fe, Al, Si, *etc*. in the aqueous solution (Oelkers, 2001). The minus prefix refers to dissolution reaction.

This study provides experiments of multi-oxide silicate mineral dissolution in water at high temperatures. A series of experiments of pyroxene dissolution in water, using a flow-through experimental reactor (Mixed flow reactor), in an open-system configuration at temperatures up to 374 °C and at 23 MPa, were performed. These experiments suggest that hydration of Si-O-Si bond and $M_i^{Zi+} - Z_i\, H^+$ exchange reaction at $T < 300$ °C are different from those at $T > 300$ °C. The dissolution rates and dissolution stoichiometry are affected by temperature, particularly above 300 °C.

3. Experimental approach

3.1. Preparation

Hedenbergitic clinopyroxene was collected on Elba Island, Rio Marina skarns (Jiang C.J., 1993, the report contains many additional references). Pure minerals were identified and selected under microscope. Mineral grains were cleaned ultrasonically in acetone to remove fine particles, rinsed with distilled water, and dried at 70–80 °C. We used specific size fraction for experiments: 20–40 mesh fraction. Surface areas of representative samples were measured with a single point BET method, using Ar-He as the absorbed gas. For the 20–40 mesh fraction, the surface area is 1.978 m^2/g for fresh pyroxene, 0.5584 m^2/g after reaction with water. The total mass of mineral placed in the mixed flow reactor is 5 g. Chemical analysis of pyroxene (Tables 1 and 2) indicates that its composition is near $Hed_{70}Di_{30}$, with minor amounts of Mn, Al, Na, K and Ti. The stoichiometric ratios of metals to Si in the pyroxene

Table 1. Chemical composition of pyroxene.

SiO_2	TiO_2	Al_2O_3	Fe_2O_3	FeO	MgO	CaO	Na_2O	K_2O	H_2O+	P_2O_5	MnO	CO_2	Σ
48.86	0.01	1.44	1.89	18.61	5.02	21.70	0.53	0.06	0.90	0.01	0.71	0.29	100.03

The pyroxene listed in Table 1 is analyzed by ICP-MS analysis, except for H_2O and CO_2. Relative standard deviation is 3–5 %.

Table 2. Stoichiometric ratios (N*i*) in pyroxene.

Ca/Si	Mg/Si	Al/Si	Fe/Si	Na/Si
0.4754	0.15397	0.014438	0.34609	0.020962

are given in Table 2. The empirical formula of the pyroxene is $(Ca_{0.95}Na_{0.04}Al_{0.01})Mg_{0.3}Fe_{0.7}(Si_{1.97}Al_{0.03})_{\Sigma=2}O_6$, when normalized to six oxygens.

3.2. Methods

A continuously stirred tank reactor (CSTR) was used to carry out the dissolution experiments in aqueous solutions, at temperatures from 25 °C to 374 °C and 23 MPa. The experimental method has been reported before (Dove & Crerar, 1990; Zhang *et al.,* 1990; Zhang *et al.,* 2000, 2002; Dove, 1999). The CSTR system, as reported in Zhang *et al.* (1990), consists of a titanium alloy pressure vessel (V = 196 ml), a liquid pump and a back pressure regulator.

In each run, the flow rate, the input solution parameters (*e.g*. pH) and the temperature were held constant for several hours, until steady-state conditions were reached. Before sampling the output solution, *i.e*. before measuring dissolution rates, the output solution was analyzed using ICP-MS at regular time interval (1 hour) at fixed conditions. Thus we know how much time is required for the attainment of 'steady' state, corresponding to the different flow rates, and when the concentrations of M_i are stable. We have tested the attainment of the steady-state dissolution, when the average resident time is changed from 54 to 230 min (flow rate: 3.66 to 0.85 ml/min) (see Table 3). For measuring steady-state dissolution rates, sampling the output solution began after attainment of steady state of the mineral-water system, which was also checked by recording the conductivity of the output solution and analyzing the composition of effluent fluids with time (for more details, see Zhang *et al.* (2006) and Appendix 1).

Experiments under steady-state conditions were conducted at temperatures of 20 °C, 100 °C, 200 °C, 260 °C, 300 °C, 350 °C and 374 °C, all under 23 MPa pressure, and at flow rates varying between 0.8 ml/min and 3.65 ml/min. In these experiments, temperature and pressure are usually maintained constant and the flow rate is changed. The mass flow rate of the inlet fluids was obtained by measuring the mass of outlet fluid for a given time interval (*i.e*., mass/Δt). At the start of a new run, the CSTR was conditioned by flowing water at room temperature for 1–2 days in order to eliminate any high energy surface (Petrovich, 1981; Chou & Wollast, 1984; Dove & Crerar, 1990; Zhang *et al.,* 1990; Nagy & Lasaga, 1992; Knauss *et al.,* 1993; Nagy, 1995). When the flow rate is changed, the system needs at least one hour to reach a new steady state again (for the used stirred flow reactor with high stirring rates). For a given series of experiments, the temperatures and the flow rates were systematically changed. Samples of effluent fluids were taken at constant values of flow rate, temperature and pressure, for a fixed surface area of mineral sample in the vessel.

The composition of the input solution is changed between the runs. The output solutions are analyzed using ICP-OES (IRIS) and ICP-MS (Excell TZA), for all dissolved metal species. The compositions of the inlet solutions are listed in Table 3. Analytical limit (Detection limit, DL) is 10 ppb (ICP-MS) or 0.01 ppb (ICP-OES), and relative standard deviation (RSD) is 5 %.

The pH of the outlet solution is measured at 25 °C within a few hours after sampling, using a HANNA HI4212 pH meter. The electrode is calibrated with HANNA buffer solution standards at pH 4.01, 6.86 and 10.0 with an average error less than ±0.01 pH units; pH values at elevated temperature are calculated, using the HCh program (Shvarov, 1989), based on the pH measured at 25 °C, and the bulk molar concentrations of aqueous Si, Mg, Ca, Fe (minor concentrations of Na, K, Al are included). The relative error on pH is estimated at about 5 %.

In this flow-through experimental reactor, the dissolution rate of the mineral (in mol/min/m^2 or mol/s/cm^2) is calculated from the relation:

$$\text{Rate} = \frac{(C_i - C_0)u}{v_i A}. \tag{5}$$

where C_i is the total output concentration (mol/L) of species i, C_0 its initial concentration, A is the total reactive surface area of the mineral (m^2), and u = V/t is the flow velocity (ml/min), where t is the average fluid residence time (min) and V the volume of the pressure vessel (ml), *i.e*. the liquid volume in the vessel; υ_i refers to the stoichiometric number of moles of the i^{th} element in one mole of pyroxene.

Equation (5) is valid for mineral dissolution rates in the case of a flow-through experiment and is similar to equations reported in other flow-through experiments (Dove & Crerar, 1990, Zhang *et al.,* 1990; 1992; Dove, 1999).

4. Experimental results

In general, the pyroxene dissolution can be described by the following overall reaction:

$$\begin{aligned} &Ca(Mg,Fe)(Si)_2O_6(s) + 2H_2O + 4H^+ \\ &\quad = Ca^{2+} + (Mg,Fe)^{2+} + 2H_4SiO_4(aq) \end{aligned} \tag{6a}$$

In the present case, the overall reaction is:

$$\begin{aligned} &(Ca_{0.95}Na_{0.04}Al_{0.01})Mg_{0.3}Fe_{0.7}(Si_{1.97}Al_{0.03})_{\Sigma=2}O_6(s) \\ &\quad + 2H_2O + 4H^+ \\ &= (Ca^{2+}_{0.95}, Na^{+}_{0.04}, Al^{3+}_{0.01}) + 0.3Mg^{2+} + 0.7Fe^{2+} \\ &\quad + 2H_4(Si,Al)O_4(aq) \end{aligned} \tag{6b}$$

Table 3. Measured compositions of effluent fluids for steady-state pyroxene dissolution (P = 23 MPa, mass put in vessel = 5 g, SA = 1.878 m^2/g, V = 196 ml.

A. Pyroxene in HCl-H_2O at 25°C

Sequence	Group A	*u* ml/min	Aver *t* min	pH	*T* °C	*m*(Si) $\times10^{-5}$	*m*(Na) $\times10^{-5}$	*m*(Mg) $\times10^{-5}$	*m*(Al) $\times10^{-5}$	*m*(K) $\times10^{-5}$	*m*(Ca) $\times10^{-5}$	*m*(Fe) $\times10^{-5}$
P1-1	1	0.87	225.14	6.75	25	10.229*	458.043	0.463	0.034	2.849	1.202	1.270
P1-2		0.88	221.72	6.7	25	2.969	390.013	0.698	0.728	1.199	1.654	1.137
P1-3		0.85	229.35	6.68	25	2.579	294.387	0.658	0.021	0.725	1.348	0.864
P1-4	2	1.17	168.24	6.62	25	2.150	205.835	1.544	0.016	0.727	3.188	0.725
P1-5		1.18	166.48	6.57	25	2.248	199.113	1.679	0.040	0.824	3.555	0.751
P1-6		1.12	175.77	6.5	25	2.250	199.774	1.835	0.018	1.288	3.998	0.741
P1-7	3	1.45	135.62	6.43	25	4.125	126.965	0.850	0.010	1.059	2.235	0.397
P1-8		1.49	131.89	6.38	25	18.996*	128.826	0.807	0.029	0.844	2.123	0.422
P1-9		1.48	132.41	6.33	25	1.164	117.822	0.670	0.115	0.952	1.812	0.348
P1-10	4	1.77	110.74	6.23	25	1.920	78.204	0.420	0.005	1.465	1.231	0.234
P1-11		1.74	112.38	6.23	25	0.889	76.574	0.450	0.006	1.296	1.276	0.244
P1-12		1.74	112.72	6.22	25	1.761	92.483	0.501	1.213	1.198	1.443	0.273
P1-13	5	2.05	95.80	6.15	25	0.954	67.113	0.308	0.005	1.062	1.080	0.192
P1-14		1.99	98.60	6.15	25	3.262	65.474	0.322	6.974	1.082	1.016	0.744
P1-15		2.03	96.48	6.12	25	0.839	69.957	0.332	0.201	3.021	1.074	0.224
P1-16	6	0.89	219.59	6.12	25	0.998	99.013	0.405	0.010	3.300	1.322	0.186
P1-17		0.89	221.38	6.1	25	1.116	96.617	0.361	0.005	2.562	1.249	0.196
P1-18		0.90	218.49	6.1	25	1.349	94.557	0.387	0.005	0.804	1.288	0.193
P1-19	7	1.17	168.12	6.15	25	1.414	85.883	0.333	0.004	0.740	1.329	0.201
P1-20		1.15	170.07	6.18	25	2.066	71.817	0.285	0.002	1.049	1.121	0.125
P1-21		1.18	166.47	6.09	25	5.493	84.504	0.328	0.006	0.997	1.386	0.186
P1-22	8	1.47	133.20	6.18	25	1.383	60.048	0.255	0.173	0.457	1.301	0.158
P1-23		1.49	131.93	6.2	25	1.570	60.409	0.254	0.005	1.104	1.370	0.171
P1-24		1.48	132.56	6.18	25	1.572	71.470	0.312	0.005	2.690	1.645	0.163
P1-25	9	1.76	111.36	6.2	25	2.321	59.148	0.280	0.005	0.843	1.679	0.115
P1-26		1.71	114.80	6.19	25	15.611*	57.830	0.259	0.009	9.674	1.701	0.156
P1-27		1.74	112.41	6.25	25	1.500	60.039	0.261	0.006	0.605	1.770	0.160
P1-28	10	2.04	96.27	6.26	25	2.871	54.383	0.291	1.298	0.521	1.845	0.238
P1-29		2.04	96.02	6.36	25	3.052	56.130	0.246	0.003	5.644	2.005	0.130
P1-30		2.05	95.68	6.35	25	1.573	53.796	0.245	0.005	4.521	2.089	0.116
P1-31	11	0.97	203.02	6.24	25	1.620	53.713	0.434	0.007	0.926	3.063	0.036
P1-32		0.79	248.82	6.2	25	1.624	53.213	0.475	2.971	1.322	3.248	0.359
P1-33		1.00	196.11	6.08	25	1.643	53.096	0.449	0.006	1.078	3.220	0.033
P1-34	12	1.16	168.91	5.98	25	3.499	55.174	0.606	0.009	0.848	6.358	0.064
P1-35		1.16	169.58	5.67	25	3.303	54.061	0.685	1.011	1.015	7.190	0.030
P1-36		1.17	168.11	5.35	25	3.550	51.283	0.603	0.017	2.095	7.338	0.016

B. Pyroxene in HCl-H_2O at 260°C

sequence	group B	*u* ml/min	Aver *t* min	pH	*T* °C	*m*(Si) $\times10^{-5}$	*m*(Na) $\times10^{-5}$	*m*(mg) $\times10^{-5}$	*m*(Al) $\times10^{-5}$	*m*(K) $\times10^{-5}$	*m*(Ca) $\times10^{-5}$	*m*(Fe) $\times10^{-5}$
P1-76	1	1.75	111.83	3.85	260	90.596	6.061	9.846	0.240	3.241	41.345	11.523
P1-77		1.86	105.44	3.91	260	91.118	5.870	9.746	0.240	2.238	40.960	7.284
P1-78		1.79	109.57	3.95	260	88.436	5.461	9.146	0.185	3.067	41.110	4.473
P1-79	2	2.37	82.71	4.62	260	63.843	3.069	3.268	0.058	10.951	25.833	0.233
P1-80		2.19	89.46	4.72	260	55.007	2.930	2.553	0.784	1.716	21.255	0.223
P1-81		2.51	78.13	4.85	260	62.893	2.990	2.834	3.400	1.880	24.815	0.228
P1-82	3	2.80	70.04	5.48	260	43.904	2.008	0.660	0.047	6.454	14.095	0.041
P1-83		2.98	65.82	5.46	260	43.079	2.371	0.616	0.054	1.768	13.123	0.084
P1-84		3.08	63.69	5.64	260	39.975	1.596	0.530	0.124	1.287	12.533	0.073
P1-85	4	3.06	64.06	6	260	26.586	0.790	0.093	0.056	0.856	5.810	0.052
P1-86		3.25	60.30	5.97	260	24.039	1.094	0.096	0.023	1.301	5.285	0.024
P1-87		3.59	54.64	5.86	260	26.250	0.753	0.092	0.019	0.920	5.388	0.019
P1-88	5	2.12	92.51	6.19	260	23.218	2.329	0.049	0.354	0.805	4.328	0.059
P1-89		1.98	99.13	6.14	260	24.393	3.380	0.048	0.019	1.472	4.643	0.020
P1-90		1.59	123.15	5.81	260	24.332	3.820	0.048	0.011	1.447	4.335	0.015

Table 3. Continued.

B. Pyroxene in HCl-H_2O at 260°C

	group	*u*	Aver *t*		*T*	*m*(Si)	*m*(Na)	*m*(mg)	*m*(Al)	*m*(K)	*m*(Ca)	*m*(Fe)
sequence	B	ml/min	min	pH	°C	$\times10^{-5}$	$\times10^{-5}$	$\times10^{-5}$	$\times10^{-5}$	$\times10^{-5}$	$\times10^{-5}$	$\times10^{-5}$
P1-91	6	2.12	92.64	6.5	260	21.857	8.761	0.037	0.020	0.594	4.205	0.008
P1-92		2.08	94.20	6.48	260	22.918	9.548	0.045	0.149	0.887	4.420	0.019
P1-93		2.40	81.67	6.44	260	21.575	9.617	0.047	0.013	0.955	4.198	0.009
P1-94	7	2.58	75.99	6.53	260	19.411	12.639	0.044	0.018	0.709	4.258	0.010
P1-95		2.62	74.76	6.53	260	19.900	12.787	0.073	3.603	0.609	4.240	0.500
P1-96		3.02	64.97	6.5	260	18.332	12.583	0.037	0.017	0.641	4.165	0.008
P1-97	8	2.93	66.91	6.55	260	17.411	14.204	0.054	0.046	0.551	4.330	0.009
P1-98		2.98	65.76	6.51	260	16.793	14.883	0.036	0.172	0.906	4.368	0.023
P1-99		3.30	59.31	6.4	260	16.954	14.783	0.039	0.015	0.964	4.420	0.005

C. Pyroxene in H_2O at temperatures from 100 to 374 °C

	group	*u*	Aver *t*		*T*	*m*(Si)	*m*(Na)	*m*(mg)	*m*(Al)	*m*(K)	*m*(Ca)	*m*(Fe)
sequence	C	ml/min	min	pH	°C	$\times10^{-5}$	$\times10^{-5}$	$\times10^{-5}$	$\times10^{-5}$	$\times10^{-5}$	$\times10^{-5}$	$\times10^{-5}$
P1-136		3.61	54.35	4.85	100	28.879	6.261	4.400	0.154	4.164	10.188	1.715
P1-137		2.87	68.37	4.9	100	28.139	6.222	4.329	0.145	4.179	9.793	1.605
P1-138		2.82	69.47	5.08	100	27.386	5.970	4.221	0.019	4.144	10.098	1.001
P1-139		3.50	55.99	5.48	100	18.804	3.044	2.256	0.008	5.128	5.628	0.780
P1-140		3.35	58.55	5.32	100	20.825	3.367	2.436	0.077	5.392	5.925	0.793
P1-141		3.37	58.19	5.51	100	17.907	2.719	2.218	0.009	5.072	5.658	0.926
P1-142		3.05	64.21	5.31	200	76.214	1.637	0.463	0.068	5.846	8.340	1.211
P1-143		2.80	69.89	5.39	200	75.500	1.597	0.457	0.147	4.085	8.325	0.934
P1-144		3.23	60.60	5.27	200	73.357	1.567	0.368	0.058	5.231	8.125	0.901
P1-145		3.36	58.39	5.31	200	58.250	1.342	0.315	0.400	4.577	8.573	0.773
P1-146		3.59	54.55	5.43	200	55.857	1.302	0.421	0.053	4.479	9.285	0.692
P1-147		2.92	67.21	5.22	200	51.464	0.969	0.272	0.090	3.459	8.108	0.721
P1-148		3.48	56.29	4.78	300	97.286	1.845	0.167	0.108	8.113	3.575	0.772
P1-149		2.34	83.82	4.93	300	91.143	2.008	0.446	0.909	5.595	4.860	0.682
P1-150		2.50	78.36	4.81	300	90.964	1.669	0.162	0.093	6.254	3.300	0.649
P1-151		3.61	54.23	4.84	300	64.857	1.306	0.183	0.074	4.015	2.525	0.636
P1-152		3.39	57.80	4.86	300	60.500	1.186	0.203	0.072	3.285	2.668	0.614
P1-153		3.42	57.33	4.89	300	58.286	1.133	0.129	0.072	3.410	2.292	0.512
P1-154		2.92	67.10	5.06	350	47.214	1.387	0.106	0.060	3.200	1.148	0.485
P1-155		2.91	67.38	5.24	350	45.036	1.133	0.121	0.050	5.387	1.122	0.583
P1-156		2.87	68.23	5.38	350	48.607	1.649	0.310	0.021	2.381	1.916	0.458
P1-157		3.29	59.62	5.19	350	43.250	1.233	0.088	0.034	3.485	0.751	0.388
P1-158		3.41	57.41	5.07	350	43.571	2.418	0.094	0.043	5.182	0.961	0.408
P1-159		3.40	57.58	5.21	350	43.429	1.200	0.082	0.043	1.943	0.811	0.406
P1-160		2.80	70.08	5.2	374	39.321	1.256	0.088	0.033	1.794	0.474	0.357
P1-161		2.92	67.14	5.43	374	39.429	8.191	0.242	0.001	2.534	0.744	0.302
P1-162		2.91	67.37	6.66	374	44.714	24.900	7.504	0.004	4.887	15.445	0.346
P1-163		3.66	53.60	5.46	374	36.179	1.378	0.089	0.028	2.921	0.635	0.425
P1-164		3.32	58.98	5.28	374	34.093	0.997	0.087	0.011	1.850	0.535	0.352
P1-165		2.73	71.71	5.34	374	36.857	1.010	0.129	0.001	3.336	0.556	0.245

Note: *only reference data due to analytical error.

4.1. Dissolution rates of pyroxene in pure water

While maintaining pure water input, the temperatures were varied from 25 to 374 °C, then steady-state dissolution rates of pyroxene were measured as a function of temperature and flow rate. The steady state outlet solutions were analysed after the experiments of pyroxene dissolution and the concentrations of all dissolving aqueous species in the solution was obtained (Table 3).

Reaction rates were calculated from the measured chemical composition of aqueous aliquots based on equation (5), corresponding to the reaction for each element released from the mineral surface. See Table 4.

The speciation of aqueous metals in the effluent solutions and the reaction equilibrium of Eq(6) were calculated from the chemical composition of the outlet solution using HCh software (Shvarov, 1989) and SUPCRT92 (Johnson *et al.,* 1992). Based on reaction (6b), the Gibbs free energy change for the $Di_{30}Hed_{70}$ – H_2O reaction at elevated temperatures is calculated from

$$\Delta G_r = RT\ \ln(Q/K) \tag{7}$$

Table 4. Measured steady-state pyroxene dissolution rate.

A. Pyroxene in HCl-H_2O at 25°C

	log *r*(Si) (m/cm^2/s)	log *r*(Na)	log *r*(Mg)	log *r*(Al)	log *r*(*K*)	log *r*(Ca)	log *r*(Fe)	log(*Q*/*K*)	ΔG_r(kcal/m)
P1-1	−10.75	−9.09	−12.09	−13.23	−11.30	−11.68	−11.65	31.48	76.82
P1-2	−11.28	−9.16	−11.90	−11.89	−11.67	−11.53	−11.69	30.03	73.28
P1-3	−11.35	−9.29	−11.94	−13.44	−11.90	−11.63	−11.83	29.26	71.39
P1-4	−11.30	−9.32	−11.44	−13.42	−11.77	−11.13	−11.77	29.37	71.67
P1-5	−11.27	−9.33	−11.40	−13.03	−11.71	−11.07	−11.75	29.35	71.61
P1-6	−11.30	−9.35	−11.38	−13.40	−11.54	−11.05	−11.78	29.35	71.61
P1-7	−10.92	−9.43	−11.61	−13.52	−11.51	−11.19	−11.94	28.46	69.43
P1-8	−10.24	−9.41	−11.62	−13.06	−11.60	−11.20	−11.90	29.47	71.91
P1-9	−11.46	−9.45	−11.70	−12.47	−11.55	−11.27	−11.98	26.63	64.97
P1-10	−11.16	−9.55	−11.82	−13.78	−11.28	−11.36	−12.08	26.13	63.75
P1-11	−11.50	−9.57	−11.80	−13.64	−11.34	−11.35	−12.07	25.46	62.12
P1-12	−11.21	−9.49	−11.76	−11.37	−11.38	−11.30	−12.02	26.21	63.95
P1-13	−11.40	−9.56	−11.90	−13.67	−11.36	−11.35	−12.10	24.72	60.31
P1-14	−10.88	−9.58	−11.89	−10.55	−11.36	−11.39	−11.53	26.36	64.33
P1-15	−11.46	−9.54	−11.87	−12.08	−10.91	−11.36	−12.04	25.05	61.13
P1-16	−11.75	−9.75	−12.14	−13.76	−11.23	−11.62	−12.47	25.49	62.20
P1-17	−11.70	−9.76	−12.19	−14.04	−11.34	−11.65	−12.45	25.34	61.82
P1-18	−11.61	−9.77	−12.16	−14.01	−11.84	−11.63	−12.46	25.02	61.06
P1-19	−11.48	−9.69	−12.11	−14.03	−11.76	−11.51	−12.33	25.15	61.37
P1-20	−11.32	−9.78	−12.18	−14.29	−11.61	−11.58	−12.54	25.33	61.80
P1-21	−10.88	−9.70	−12.11	−13.85	−11.63	−11.48	−12.36	26.19	63.91
P1-22	−11.39	−9.75	−12.12	−12.29	−11.87	−11.41	−12.33	24.66	60.17
P1-23	−11.33	−9.74	−12.12	−13.83	−11.48	−11.39	−12.29	25.29	61.71
P1-24	−11.33	−9.67	−12.03	−13.87	−11.10	−11.31	−12.31	25.82	63.00
P1-25	−11.08	−9.68	−12.00	−13.74	−11.52	−11.22	−12.39	25.46	62.13
P1-26	−10.27	−9.70	−12.05	−13.53	−10.48	−11.23	−12.27	28.23	68.88
P1-27	−11.28	−9.68	−12.04	−13.67	−11.67	−11.21	−12.25	25.28	61.68
P1-28	−10.93	−9.65	−11.92	−11.27	−11.67	−11.12	−12.01	26.02	63.48
P1-29	−10.90	−9.64	−11.99	−13.95	−10.63	−11.08	−12.27	27.22	66.41
P1-30	−11.19	−9.65	−11.99	−13.69	−10.73	−11.06	−12.32	26.45	64.54
P1-31	−11.50	−9.98	−12.07	−13.87	−11.74	−11.22	−13.15	25.26	61.63
P1-32	−11.59	−10.07	−12.12	−11.33	−11.68	−11.29	−12.24	26.31	64.20
P1-33	−11.48	−9.97	−12.04	−13.93	−11.66	−11.19	−13.17	24.69	60.25
P1-34	−11.09	−9.89	−11.85	−13.69	−11.70	−10.83	−12.83	25.57	62.38
P1-35	−11.11	−9.90	−11.80	−11.63	−11.63	−10.78	−13.15	24.13	58.87
P1-36	−11.08	−9.92	−11.85	−13.39	−11.31	−10.76	−13.44	22.87	55.80

B. Pyroxene in HCl–H_2O at 260°C

	log *r*(Si) (m/cm^2/s)	log *r*(Na)	log *r*(Mg)	log *r*(Al)	log *r*(*K*)	log *r*(Ca)	log *r*(Fe)	log(*Q*/*K*)	ΔG_r/1000
P1-76	−9.49	−10.67	−10.46	−12.07	−10.94	−9.84	−10.39	−19.47	−47.51
P1-77	−9.47	−10.66	−10.44	−12.05	−11.08	−9.81	−10.56	−19.61	−47.84
P1-78	−9.50	−10.71	−10.48	−12.18	−10.96	−9.83	−10.79	−19.61	−47.84
P1-79	−9.52	−10.83	−10.81	−12.56	−10.28	−9.91	−11.95	−18.84	−45.97
P1-80	−9.61	−10.89	−10.95	−11.46	−11.12	−10.03	−12.01	−19.60	−47.84
P1-81	−9.50	−10.82	−10.84	−10.76	−11.02	−9.90	−11.94	−18.80	−45.87
P1-82	−9.61	−10.95	−11.43	−12.57	−10.44	−10.10	−12.63	−17.85	−43.55
P1-83	−9.59	−10.85	−11.43	−12.49	−10.97	−10.10	−12.30	−18.19	−44.38
P1-84	−9.61	−11.00	−11.48	−12.11	−11.10	−10.11	−12.34	−17.99	−43.89
P1-85	−9.78	−11.31	−12.24	−12.46	−11.28	−10.45	−12.49	−18.62	−45.43
P1-86	−9.80	−11.14	−12.20	−12.82	−11.07	−10.46	−12.81	−18.88	−46.06
P1-87	−9.72	−11.26	−12.18	−12.86	−11.18	−10.41	−12.86	−19.65	−47.95
P1-88	−10.00	−11.00	−12.68	−11.82	−11.46	−10.73	−12.60	−17.89	−43.66
P1-89	−10.01	−10.87	−12.72	−13.12	−11.23	−10.73	−13.11	−18.08	−44.11
P1-90	−10.11	−10.91	−12.81	−13.47	−11.33	−10.86	−13.33	−19.52	−47.62
P1-91	−10.03	−10.43	−12.81	−13.06	−11.60	−10.75	−13.46	−17.26	−42.11
P1-92	−10.02	−10.40	−12.72	−12.20	−11.43	−10.73	−13.10	−16.61	−40.52
P1-93	−9.98	−10.33	−12.64	−13.19	−11.34	−10.69	−13.38	−17.13	−41.79
P1-94	−10.00	−10.18	−12.65	−13.04	−11.43	−10.65	−13.29	−16.84	−41.09

Table 4. Continued.

B. Pyroxene in HCl–H_2O at 260°C

	log r(Si) (m/cm^2/s)	log r(Na)	log r(Mg)	log r(Al)	log r(*K*)	log r(Ca)	log r(Fe)	log(*Q*/*K*)	ΔG_r(kcal/m)
P1-95	−9.98	−10.17	−12.41	−10.72	−11.49	−10.65	−11.58	−14.95	−36.48
P1-96	−9.95	−10.12	−12.65	−12.98	−11.41	−10.60	−13.34	−17.25	−42.10
P1-97	−9.99	−10.08	−12.50	−12.57	−11.49	−10.59	−13.27	−16.84	−41.10
P1-98	−10.00	−10.05	−12.67	−11.99	−11.26	−10.58	−12.87	−16.58	−40.46
P1-99	−9.95	−10.01	−12.58	−12.99	−11.19	−10.53	−13.52	−17.64	−43.03

C. Pyroxene in H2O at temperatures from 100 to 374°C

sequence	log r(Si) (m/cm^2/s)	log r(Na)	log r(Mg)	log r(Al)	log r(K)	log r(Ca)	log r(Fe)	log(*Q*/*K*)	ΔG_r/1000
P1-136	−9.68	−10.34	−10.49	−11.95	−10.52	−10.13	−10.90	−53.71	−91.73
P1-137	−9.79	−10.44	−10.60	−12.08	−10.62	−10.25	−11.03	−53.79	−91.86
P1-138	−9.81	−10.47	−10.62	−12.97	−10.63	−10.24	−11.24	−54.04	−92.28
P1-139	−9.88	−10.67	−10.80	−13.25	−10.44	−10.40	−11.26	−55.20	−94.26
P1-140	−9.85	−10.64	−10.78	−12.28	−10.44	−10.40	−11.27	−54.98	−93.89
P1-141	−9.91	−10.73	−10.82	−13.21	−10.46	−10.42	−11.20	−55.22	−94.31
P1-142	−9.33	−11.00	−11.55	−12.38	−10.44	−10.29	−11.13	−53.95	−116.82
P1-143	−9.37	−11.04	−11.59	−12.08	−10.64	−10.33	−11.28	−54.24	−117.46
P1-144	−9.32	−10.99	−11.62	−12.42	−10.47	−10.28	−11.23	−54.29	−117.56
P1-145	−9.40	−11.04	−11.67	−11.57	−10.51	−10.24	−11.28	−54.73	−118.50
P1-146	−9.39	−11.03	−11.52	−12.42	−10.49	−10.17	−11.30	−54.67	−118.39
P1-147	**−9.52**	**−11.24**	**−12.8**	**−12.28**	**−10.69**	**−10.32**	**−11.37**	**−55.22**	−119.56
P1-148	**−9.17**	−10.89	−11.93	−12.12	−10.24	−10.60	−11.27	−51.79	−135.86
P1-149	**−9.37**	−11.02	−11.68	−11.37	−10.58	−10.64	−11.49	−51.47	−135.01
P1-150	**−9.34**	−11.07	−12.09	−12.33	−10.50	−10.78	−11.48	−52.13	−136.75
P1-151	**−9.33**	−11.02	−11.87	−12.27	−10.53	−10.73	−11.33	−52.80	−138.49
P1-152	**−9.38**	−11.09	−11.86	−12.31	−10.65	−10.74	−11.38	−52.93	−138.85
P1-153	**−9.40**	−11.11	−12.05	−12.30	−10.63	−10.80	−11.45	−53.31	−139.84
P1-154	**−9.56**	−11.09	−12.20	−12.45	−10.72	−11.17	−11.54		
P1-155	−9.58	−11.18	−12.15	−12.53	−10.50	−11.18	−11.47		
P1-156	−9.55	−11.02	−11.75	−12.91	−10.86	−10.95	−11.58		
P1-157	−9.54	−11.09	−12.23	−12.65	−10.64	−11.30	−11.59		
P1-158	−9.52	−10.78	−12.19	−12.53	−10.45	−11.18	−11.55		
P1-159	−9.53	−11.08	−12.25	−12.53	−10.87	−11.25	−11.56		
P1-160	−9.65	−11.15	−12.30	−12.73	−10.99	−11.57	−11.70		
P1-161	−9.63	−10.32	−11.85	−14.28	−10.83	−11.36	−11.75		
P1-162	−9.58	−9.84	−10.36	−13.65	−10.54	−10.04	−11.69		
P1-163	−9.57	−10.99	−12.18	−12.68	−10.67	−11.33	−11.50		
P1-164	−9.64	−11.17	−12.23	−13.15	−10.91	−11.45	−11.63		
P1-165	−9.69	−11.25	−12.15	−14.26	−10.74	−11.51	−11.87		

with

$$Q = \frac{a^2_{H_4(Al,Si)O_4}\, a^{0.95}_{Ca^{2+}}\, a^{0.30}_{Mg^{2+}}\, a^{0.01}_{Al^{3+}}\, a^{0.7}_{Fe^{2+}}\, a^{0.04}_{Na^{+1}}}{a^4_{H^+}\, a^2_{H_2O}} \quad (8)$$

where K is the equilibrium constant of the reaction, Q the ion activity product and a_i the activity of aqueous species i. See Table 4.

The calculation of K does not take into account minor elements (Na, K, Mn, Ti, Fe, Al) that make about 5 % of the total cation number in the pyroxene formula.

The speciation calculations indicate that Ca^{2+}, Mg^{2+}, Fe^{2+}, H_4SiO_4, $Al(OH)_4^-$ and OH^- are the dominant aqueous species under equilibrium conditions at high temperatures (100–374 °C). The speciation calculations predict that the outlet solutions are undersaturated with respect to all possible secondary phases, which suggests there should be no secondary mineral forming on the pyroxene surface, or, there should be no precipitation of secondary minerals during pyroxene dissolution (Appendix 2, Table A).

The pyroxene surface was analyzed by SEM before and after the dissolution experiments (Table 5). Secondary mineral were rarely observed on the pyroxene surface after reaction with pure water. Figure 1a shows the columnar shape of the pyroxene grains and their smooth fresh surfaces. After reaction with pure water, the mineral surfaces show etch edges and a few secondary minerals, 10–100 nm in diameter, of Fe-oxide composition, covering less than 1 % of the surface.

The SEM analysis of pyroxene before and after a dissolution experiment (at 374 °C) indicates the

Table 5. EDAX ZAF Quantification of pyroxene reacted with water.

	Fresh pyroxene		After reaction with water (to 374 °C)			Nanoparticles on surface*	
	Surface analysis Average of 3 samples		Surface analysis Average of 3 samples			Point analysis Average of 2 samples	
Element	Wt %	At %	Wt %	At %	At % change	Wt %	At %
O	36.087	55.31	39.82	59.16	3.86	28.35	55.435
Na	0.43	0.46	0.50	0.52	0.06		
Mg	3.37	3.4	3.42	3.33	−0.07	1.9	2.445
Al	0.757	0.68	0.6	0.53	−0.15	0.545	0.635
Si	25.84	22.57	24.27	20.59	−2.02	5.965	6.645
K	0.15	0.09	0.10	0.07	−0.02	0	0
Ca	16.32	9.99	14.50	8.65	−1.34	3.715	2.895
Fe	17.06	7.49	16.36	7.047	−0.45	52.45	29.39
Other			0.42	0.11		0.42	0.185
100	100	100	100	100		99.91	*99.91

Wt% refers to weight percentage, At% is atomic numbers, At % change is compared with fresh mineral.
*Mainly iron oxide with aluminosilicate contribution because particle size is very small (10–500 nm) and background composition was involved. Other metal: Mo, or P, Ga from vessel erosions.

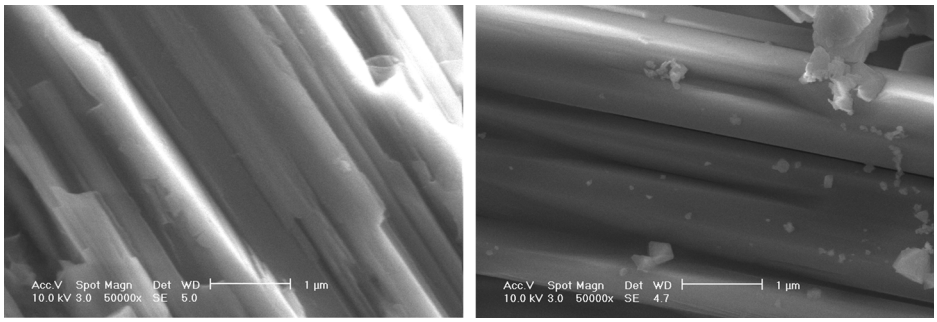

Fig. 1. Scanning electron micrographs of pyroxene surface before and after reaction with water; a, fresh; b after reaction with water.

compositional changes in atom numbers (Table 5): oxygen was added by 3.86 %, Mg was reduced by 0.07 %, Al reduced by 0.15 %; Si reduced by 2.02 %, Ca reduced by 1.34 %, Fe reduced by 0.45 %, Na added by 0.06 %. This indicates that a leached layer depleted mainly in Si and Ca occurs at the mineral surface.

4.2. Stoichiometry of pyroxene dissolution

Steady-state dissolution rates of pyroxene were measured as a function of average residence time (flow rate) and temperatures. Basically, dissolution rates are not dependent on the sample history, or the rates did not change with the elapsed time. See Appendix 1.

The general variations of the release rates of Ca, Mg, Fe, Si with temperature are shown in Fig. 2. For a given element, the release rate first increases with temperature, reaches a maximum at T_{max}, and then decreases with continued temperature increase. For Si, the maximal rate is observed at $T_{max} = 300$ °C; r_{Ca} and r_{Al} are maximal at 260 °C (T_{max}), r_{Mg} and r_{Fe} at 100 °C(T_{max}), r_{Na} is maximal at 25 °C.

In Fig. 2a dashed lines show the scattered data of the release rates of each metal M_i, caused by varying flow rates at each temperature. Reaction stoichiometry was examined by comparing release ratios of molar concentrations of $\Delta m_i/\Delta m_{Si}$ in the effluent solution with the stoichiometric numbers of moles of these elements in the pyroxene. Δm_i stands for the difference between the inlet and outlet fluid concentration of the subscripted metal i, m_{Mi}, such as Mg, Ca, Fe *etc*. When dissolution is stoichiometric, $\Delta m_i/\Delta m_{Si}$ in the effluent solution (or r_{Mi}/r_{Si}) is the same as the stoichiometric number in solid.

The stoichiometric ratios M_i/Si in the pyroxene are shown as horizontal dashed lines in Fig. 3a; M_i/Si is the ratio between molar concentrations of i and the molar concentration of Si in the solid (m_i/m_{Si} ratio in solid, *i.e*., stoichiometric number) (Tables 1 and 2).

Reaction stoichiometry was also examined by comparing r_{Mi}/r_{Si}, the ratio of the release rate of metal M_i to that of Si, with the stoichiometric ratios M_i/Si in the pyroxene. When dissolution is stoichiometric, $\Delta m_i/\Delta m_{Si}$ in the effluent solution (or r_{Mi}/r_{Si}) is the same as the stoichiometric number in solid. In brief, Fig. 3a, b indicate that Ca, Mg,

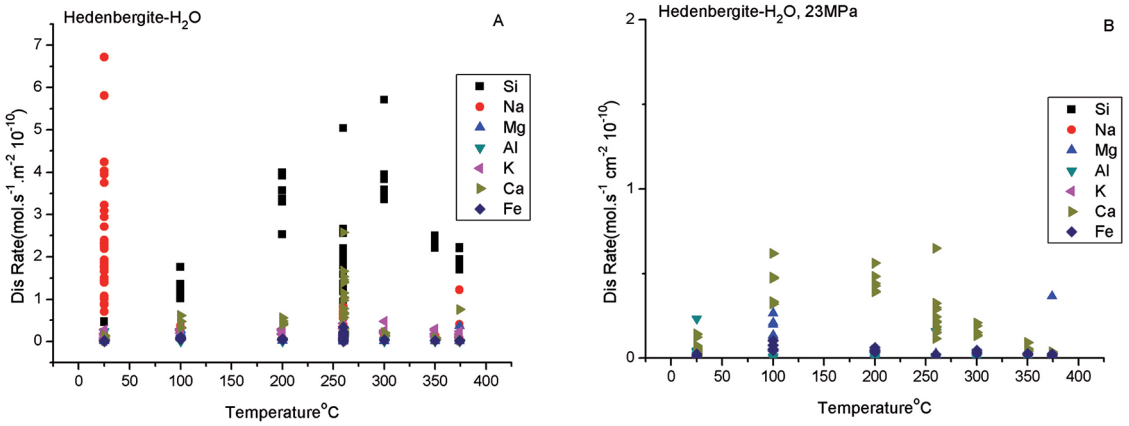

Fig. 2. Release rates *vs.* temperature for pyroxene dissolution in water at 23 MPa. The rates are given for Si, Mg, Fe, Ca, Na, K, Al. Because of overlapping data, two diagrams are provided for easier reading (Si, Na and K points are absent in Fig. 2b). The vertical alignments refer to the flow rate changed at each temperature.

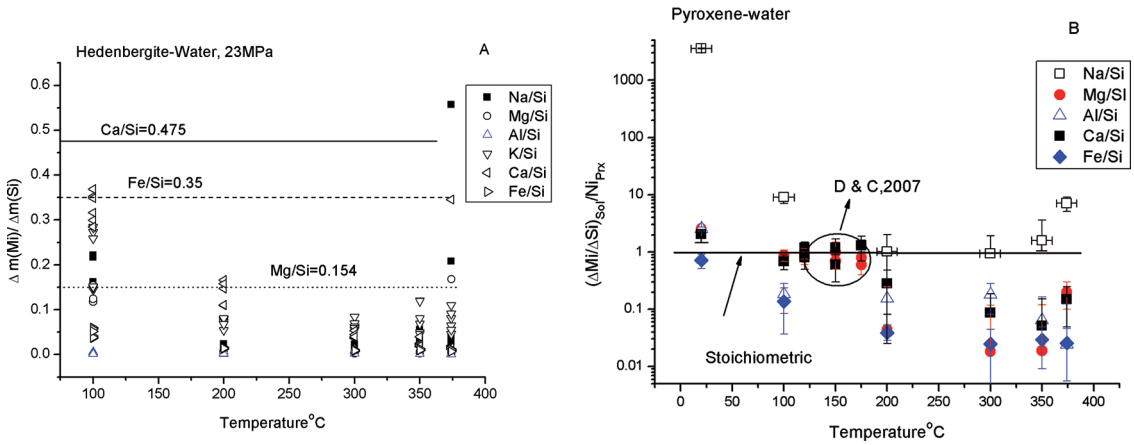

Fig. 3. (a) Release ratios $\Delta m_i/\Delta m_{Si}$ as a function of temperature for pyroxene ($Di_{30}Hed_{70}$) dissolving in water. (b) Release ratios $(\Delta m_i/\Delta m_{Si})_{sol}$ *vs.* stoichiometric number N_i in mineral as a function of temperature. Here, the $(\Delta m_i/\Delta m_{Si})_{sol}$ are the average values for each temperature. We can obtain the approximate constant value corresponding to temperature, and obtain the average values (Fig. 4). The circle allows one to compare our data with those by Dixit & Carroll (2007) for the release ratio of diopside dissolution at 120, 150 and 175 °C.

Fe, Al dissolve faster than Si in the temperature range from 25 to 100 °C because $\Delta m_i/\Delta m_{Si}$ ratios for Ca, Mg, Fe are higher than the stoichiometric numbers. As temperature increases from 200 to 374 °C, Si dissolves more easily than other elements. Figure 3 shows that $\Delta m_i/\Delta m_{Si}$ ratios in the effluent solutions vary with respect to temperature.

Ca, Mg and Fe are released easier than Si in water at 25 °C. Na is released easier in water in the temperature range from 25 to 100 °C than Si. As temperature increases from 100 to 374 °C, the release rate of Si increases faster than other element rates (Fig. 3b).

If the relative release rates were related to the experiment time length, then the $\Delta M_i/\Delta Si$ in the effluent solution would be changing with time, and not constant. Our experiments demonstrate that: the $\Delta M_i/\Delta Si$ in the effluent solution at a constant temperature is almost constant after attainment of a steady state, as we changed flow rate and also made the experiment time be longer. Figure 4a, b, c indicate that $\Delta M_i/\Delta Si$ ratios in the effluent solution for Ca, Mg, Fe, are almost constant when changing flow rates. In some cases, the $\Delta M_i/\Delta Si$ ratios in the effluent solution vary slightly with flow rates, *e.g.*, at 260 °C. When changing the flow rates at each temperature, experiments would spend 2–3 days. These experiments demonstrate that measurements of dissolution rates are at steady state. The $\Delta M_i/\Delta Si$ ratios in the effluent solution for Ca, Mg, Fe, . . . at 20 °C or at 260 °C are different from the stoichiometric number N_i (in mineral). Thus, we calculated the average values for $\Delta m_i/\Delta m_{Si}$ ratios at each temperature, (Fig. 3b). $\Delta m_{Mi}/\Delta m_{Si}$ ratios in solution are compared to the stoichiometric number M_i/Si in the solid (N_i); *i.e.*, the ratio between Ca (or Mg . . .) concentration and Si concentration at steady-state is divided by the stoichiometric number of moles of these elements in the solid; if the balance is 1, it is stoichiometric dissolution, see Fig. 3b (Oelkers & Schott, 2001; Dixit & Carroll, 2007).

Pyroxene dissolution is non-stoichiometric in pure water at most temperatures, but it becomes nearly stoichiometric

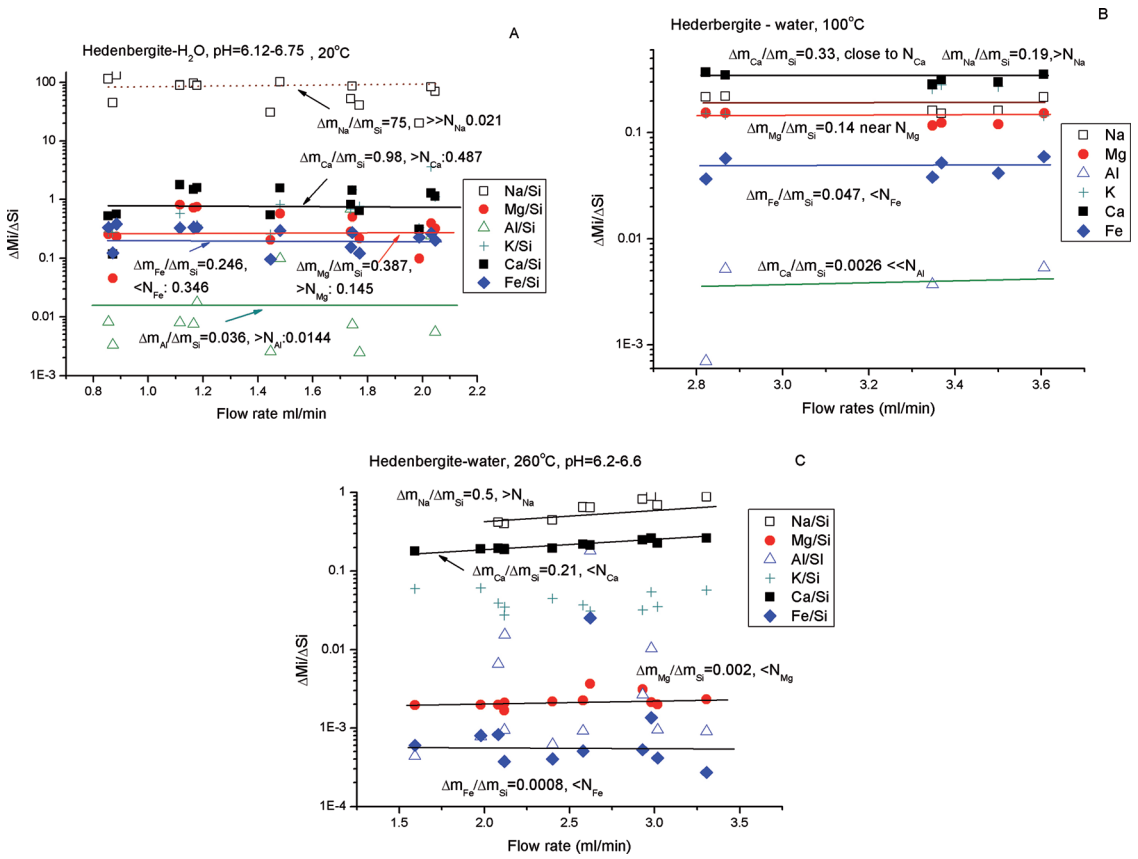

Fig. 4. Release ratios $\Delta m_i/\Delta m_{Si}$ as a function of flow rate for pyroxene ($Di_{30}Hed_{70}$) dissolution in water. a) At 25 °C. The horizontal lines show the $\Delta m_i/\Delta m_{Si}$ ratios in solution for Mg, Ca, Al and Na; they are higher than the stoichiometric numbers in solid N_i. These $\Delta m_i/\Delta m_{Si}$ ratios are stable and do not vary with flow rates. Thus the average $\Delta m_i/\Delta m_{Si}$ values can be obtained. (b) At 100 °C. The horizontal lines show the $\Delta m_i/\Delta m_{Si}$ ratios in solution for Mg, Ca, Al, Fe and Na. The ratios Mg, Ca are close to the stoichiometric numbers in solid N_i. The $\Delta m_i/\Delta m_{Si}$ ratios for Al and Fe are lower than for N_i, but are higher for Na (N_{Na}). These ratios do not vary with flow rates. (c) At 260 °C, the horizontal lines show the $\Delta m_i/\Delta m_{Si}$ ratios in solution for Mg, Ca, Fe are lower than the N_i stoichiometric ratios of the solid. Those $\Delta m_i/\Delta m_{Si}$ ratios are stable and do not strongly vary with flow rates.

at 100 °C (Fig. 3a, b and Fig. 4b). Results indicate that the $\Delta m_{Mg}/\Delta m_{Si}$ (or release rate ratios r_{Mg}/r_{Si}) are close to stoichiometric (~0.154 in solid) at 100 °C. The $\Delta m_{Mg}/\Delta m_{Si}$ and $\Delta m_{Ca}/\Delta m_{Si}$ are higher than stoichiometric numbers at 25 °C. $\Delta m_{Mg}/\Delta m_{Si}$ and $\Delta m_{Ca}/\Delta m_{Si}$ are lower than stoichiometric number at temperatures from 200 °C to 374 °C. $\Delta m_{Fe}/\Delta m_{Si}$ at temperatures from 100 °C to 374 °C are lower than their stoichiometric numbers.

Dissolutions are incongruent at 20 °C, 200 °C, 300 °C, 350 °C and 374 °C (Fig. 3b). We compare our data with those from Dixit & Carroll (2007) who reported the dissolution rates of diopside at temperatures from 120 to 175 °C (Fig. 3b). Our sample of hedenbergite-diopside solid solution is different from diopside but Ca and Mg dissolution is stoichiometric at 100 °C, which is close to the results for diopside at 120 °C (Dixit & Carroll, 2007).

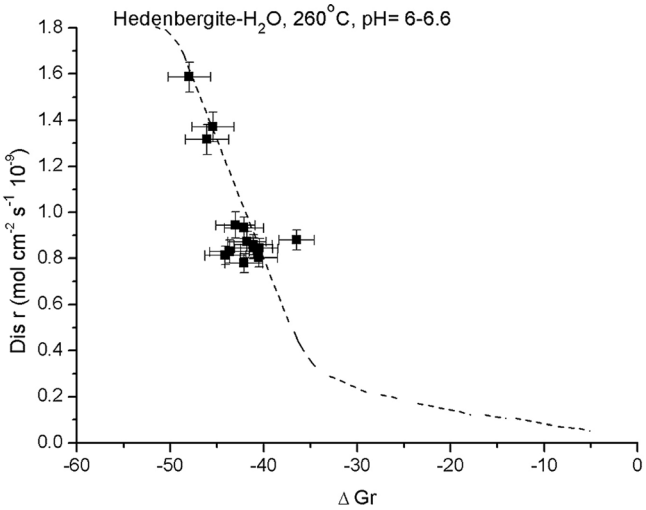

Fig. 5. The steady-state dissolution rates of pyroxene as a function of ΔG_r at 260 °C. The error bars surrounding the symbols correspond to a 4 % uncertainty of the ΔG_r data.

4.3. Effect of solution chemistry on dissolution rates

Plotting the dissolution rates (r_{Si}) in neutral aqueous solution against ΔG_r (Fig. 5) indicates that the dissolution experiments were conducted at conditions far from equilibrium. Far-from-equilibrium mineral dissolution rates have been traditionally interpreted to be a function of pH, but independent of the aqueous concentrations of the metals present in the mineral itself (*e.g.* Knauss &

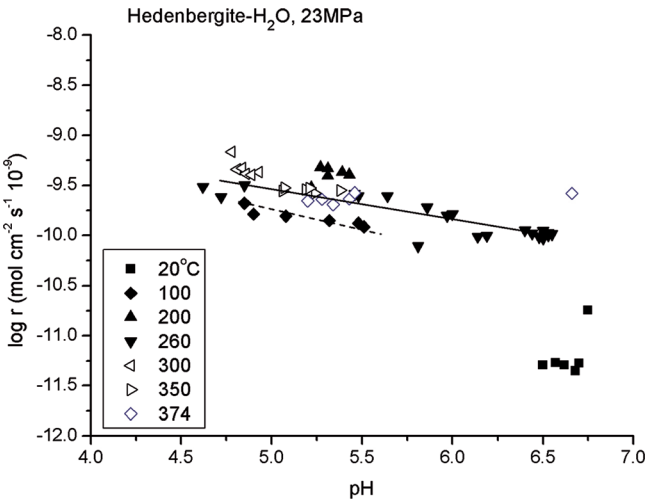

Fig. 6. Variation of the logarithm of steady-state pyroxene dissolution rates (release rates of Si) at temperatures from 25 °C to 374 °C in neutral solutions as a function of pH. The symbols correspond to experimental data reported in Table 3.

Wolery, 1986, 1989; Murphy & Helgeson, 1987, 1989; Oelkers & Schott, 2001; Zhang *et al.,* 2002). The pyroxene steady-state dissolution rates in neutral aqueous solutions measured at temperatures from 25 to 374 °C in the present study are illustrated as a function of pH in Fig. 6. Dissolution rates (release rates of Si, r_{Si}) increase with decreasing pH, and vary weakly, at near constant pH, when the concentrations of Mg, Ca and Fe in the reactive fluid are changing (Fig. 7).

It can be seen that pyroxene dissolution rates (r_{Si}) measured at 100 °C at pH range from 4.5 to 5 vary slightly with molar concentrations of aqueous Mg, Ca and Fe (Fig. 7). The dissolution rates (r_{Si}) do not change with molar concentration of aqueous species Mg, Ca and Fe at 25 °C at pH from 6.5 to 6.8. Similarly, the dissolution rates at 200 °C at pH from 4.9 to 5.5 are independent of aqueous Mg, Ca and Fe (Fig. 7). The same phenomenon also happens at 260 °C at pH from 6.2 to 6.5.

These observations are consistent with Eq. (4) and with pyroxene dissolution at neutral pH as controlled by the destruction of a precursor complex formed by M_i-proton exchange reactions (M_i refers to Mg, Ca and Fe). Thus, logarithms of pyroxene dissolution rates, measured during experiments with a constant inlet aqueous solution, appear to vary systematically with the pH of outlet fluids and logarithms of the molar concentrations of aqueous Mg, Ca and Fe (Figs. 6 and 7).

In Eq. (4), order α refers to the exponent of rate in $-r = ((a_{H^+})^{Zi}/a_{M_i}{}^{Zi+})\ \alpha$. The solid line through the data in the plot: $\log(r)$ *vs.* $\log((a_{H+})^2/a_{Mg^{2+}})$ at 100 °C has a slope of 0.165, this is the exponent value (Fig. 8). The close correspondence between the line and the symbols are consistent with $r_{Si}\ \alpha\ ((a_{H^+})^2/a_{Mg^{2+}})$. The determination coefficient (R^2) for the best fit of the data with slope 0.165 is 0.89, and $k = 10^{-9.8}$ (referring Eq. (4, 9)). Calculation of the reaction order from the slope of the line in Fig. 8 yields the α value of 0.154 and 0.16, corresponding to $\log(r)$ *vs.* $\log((a_{H^+})^2/a_{Fe^{2+}})$ and $\log(r)$ *vs.* $\log((a_{H^+})^2/a_{Ca^{2+}})$ respectively, at 100 °C. Regression calculations performed using Eq. (4) suggest that the α value for dissolution in water at 100 °C are almost identical, corresponding to Mg, Ca and Fe, plotted in Fig. 8. The slope, correlation coefficient and k values are listed in Table 6. The regression curves through the data are consistent with

$$r = k(a_H^{2+}/a_{Mg^{2+}})^{0.165},$$
$$r = k(a_H^{2+}/a_{Fe^{2+}})^{0.154}, \quad (9)$$
$$r = k(a_H^{2+}/a_{Ca^{2+}})^{0.16}$$

According to Eq (4) the exponent values refer to experimental n_i. As mentioned above, the stoichiometric number of Mg atoms in pyroxene, normalized to the formation of one Si (or one precursor complex), n_{Mg} is 0.154. Experiment at 100 °C provides data with a slope corresponding to $\log r$ *vs.* $\log((a_{H^+})^2/a_{Mg^{2+}})$ of 0.165, close to the stoichiometric number n_{Mg}. In addition, the exponent values for Mg, Ca and Fe, referring to the rate $-r = ((a_{H^+})^{zi}/a_{Mi}{}^{zi+})^{\alpha}$, are almost similar, which proves that stoichiometric dissolution of pyroxene in pure water occurs at 100 °C.

These observations are consistent with the concept that dissolution rates are controlled by the destruction of partially detached Si tetrahedra formed by the exchange of two protons for one Mg (or Fe, or Ca) near the pyroxene surface.

4.4. Temperature effects on dissolution rates

Temperature dependence on dissolution rates can be illustrated in Fig. 9 by using Arrhenius relationship as follows:

$$\text{Rate constant} = A\exp(-E_a/RT) \quad (10a)$$

where A is a pre-exponential factor (mol/m^2/s), nearly independent on temperature, E_a refers to the activation energy (kJ/mol), R stands for the gas constant, T (K) denotes the absolute temperature. Note that some scientists applied E_A, apparent activation energy, instead of E_a, see Eq. (10a) (Brady & Walther, 1992; Casey *et al.,* 1993; Oelkers & Schott, 1999). Measured dissolution rates are depicted as a function of reciprocal temperature in Fig. 9. Taking account of the definition of the apparent activation energy, E_A given by

$$E_A = -R(\partial \ln r/\partial(1/T))_{pH}, \quad (10b)$$

the slope in Fig. 9 is equal to $-E_A/R$. The straight line depicted in this figure corresponds to the apparent activation energy of 22.667 kJ/mol, which is deduced from the kinetic experiment of pyroxene dissolution in pure water at temperatures of 25–300 °C.

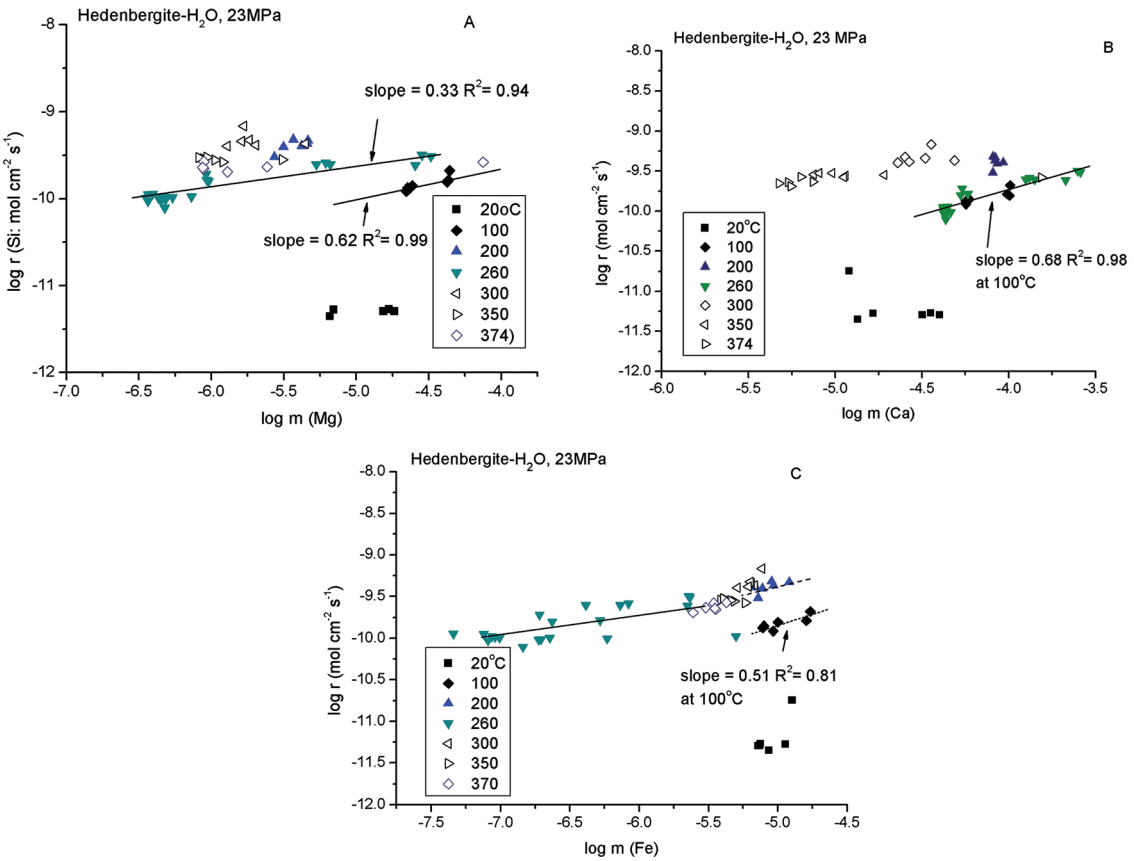

Fig. 7. Variation of the logarithm of steady-state pyroxene dissolution rates at temperatures from 25 °C to 374 °C in neutral solutions with the logarithm molar concentrations of aqueous Mg, Ca and Fe. Release rates of Si change with molar concentrations of aqueous Mg, Ca and Fe at 25 °C and pH = 4.9 to 5.5. Release rates of Si do not change with molar concentrations of aqueous Mg, Ca and Fe at 25 °C and pH = 6.5 to 6.8, at 200 °C and pH = 4.9 to 5.5 and at 260 °C and pH = 4.8 to 6.5. The symbols correspond to experimental data reported in Table 3. a) log r(Si) *vs*. log m(aqueous Mg); b) log r(Si) *vs*. log m(aqueous Ca) and c) log r(Si) *vs*. log m(aqueous Fe), respectively. The linear curve (for 100 °C) represents a least squares fit of the data; the equation and coefficient of determination (R^2) of this curve are given in the figure.

All experiments are performed in far from equilibrium conditions, where the contribution of the reverse reaction is negligible; so regression of experimental data was performed with a combination of Eq.(4) and (10), as:

$$-r_+ = A\exp(-E_A/RT)((a_{H^+})^{zi}/a_{Mi^{zi+}})^{\alpha} \quad (11)$$

Therefore, it is possible to consider all the data together and to perform a multiple linear regression so as to determine the E_A, α and A using the following relationship derived from Eq. (12):

$$\log r_+ = \log A - E_A/(2.303\,RT) + \alpha\,\log((a_{H^+})^{zi}/a_{Mi^{zi+}}) \quad (12)$$

According to the stoichiometry of pyroxene dissolution in water at 100 °C, we can do a theoretical calculation according to Eq.(12). At 100 °C, the α values for $(a_{H^+})^2/a_{Mg^{2+}}$, $(a_{H^+})^2/a_{Ca^{2+}}$ and $(a_{H^+})^2/a_{Fe^{2+}}$ are nearly the same, and equal to 0.165 (0.16–0.165), close to the stoichiometric number n_{Mg}. The α values at 100 °C are listed in Table 6, and the pre-exponential factor A was calculated as equal to 2.011 $\times 10^{-7}$ m cm^{-2} s^{-1} at 100 °C.

At high temperatures, from 300 to 374 °C, the activation energy will have an opposite sign (Fig. 9). This indicates that reaction rates will decrease with increasing temperature at temperatures > 300 °C and 23 MPa. A previous study reported that the dissolution rate of carbonate minerals decreases with increasing temperature, as derived from the effect of the enthalpy value of the protonation reaction at the mineral surface (*e.g.*, the case of magnesite, Schott *et al.,* 2009).

5. Discussion

5.1. Stoichiometric dissolution of pyroxene

Experiments indicate that stoichiometric dissolution of pyroxene occurs in pure water at 100 °C.

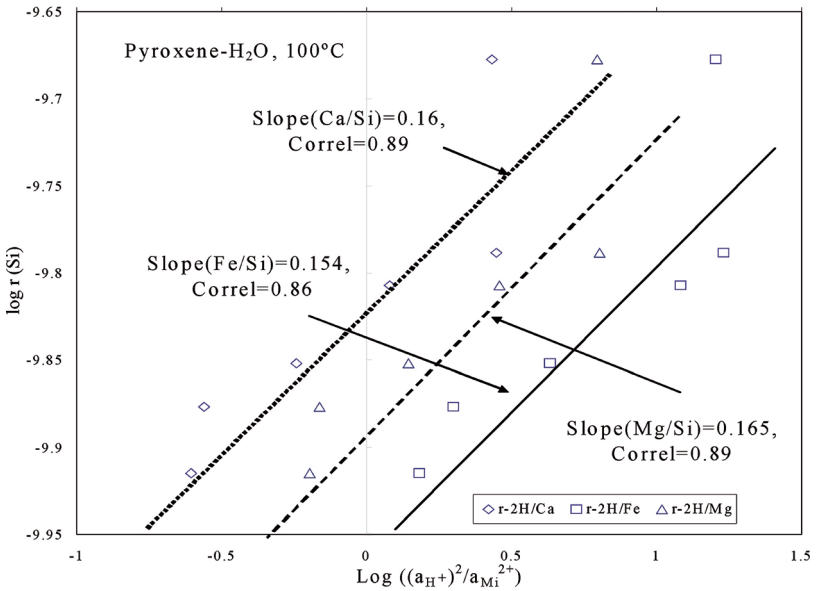

Fig. 8. Variation of the logarithm of steady-state pyroxene dissolution rates in water at 100 °C with the corresponding logarithm of $a^2_{H^+}/a_{Mi^{2+}}$. The symbols of open squares, open triangles and open diamonds refer to $2H^+ = Mg^{2+}$, $2H^+ = Ca^{2+}$ and $2H^+ = Fe^{2+}$ exchange reactions on mineral surface and correspond to experimental data reported in Tables 3 and 4. Error bars correspond to a ± 0.2 log unit estimated uncertainty of these data. The linear curve represents a fit of the data measured at pH ~ 7; the equation slope and correlation coefficient (R^2) of determination of this curve are given in the figure.

Table 6. Calculations of the parameters slope α deduced from $r(\mathrm{Si}) = k\,((a_{H^+})^{Zi}/(a_{M^{Zi+}}))^{\alpha}$ corresponding to pyroxene dissolution in water shown in Fig. 8.

100°C	slope α	R_2	intercept
log *r vs.* $\log((a_{H^+})^2/a_{Mg^{2+}})$	0.165	0.89	−9.87
log *r vs.* $\log((a_{H^+})^2/a_{Ca^{2+}})$	0.16	0.89	−9.9
log *r vs.* $\log((a_{H^+})^3/a_{Fe^{2+}})$	0.154	0.86	−9.8

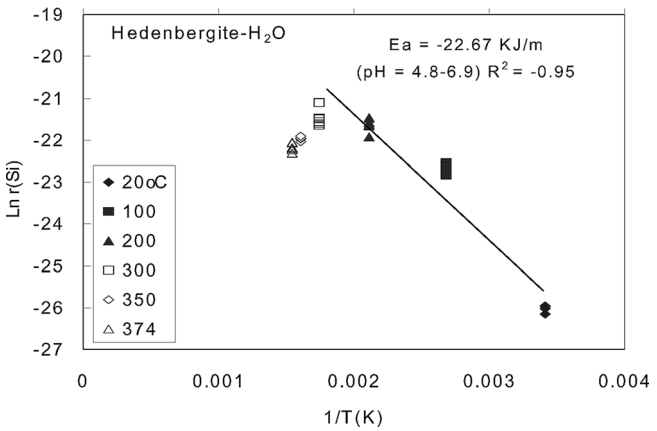

Fig. 9. Arrhenius plots illustrating the variation of measured steady-state pyroxene dissolution rates in water with temperature: variation of the logarithm of the rates for experiments performed at temperature from 25 to 374 °C depicted as a function of reciprocal temperature.

At neutral conditions, pyroxene dissolution rates observed at 100 °C are consistent with $-r = k\,((a_{H^+})^2/a_{Mi^{2+}})^{0.165}$. Experiments demonstrate that hydrogen-ion activity affects the proton-metal exchange on mineral surface.

Some insight into the origin of these behaviours may be gained from the consideration of the dissolution mechanism of other silicate minerals. A mineral which contains octahedral M_i in addition to tetrahedral Si in its structure (Devidal *et al.,* 1997; Cama *et al.,* 2000; Harouiya & Oelkers, 2004; Saldi *et al.,* 2007) has its dissolution rate controlled by precursor complexes formed by M_i for proton exchange reaction only at acid pH. At basic pH the dissolution rate of the mineral becomes dependent on aqueous Si concentration in addition to aqueous M_i concentration. This difference may stem from differences in breaking rates for octahedral M_i–O bonds *vs.* tetrahedral Si–O bonds.

Our observations combined with the previous studies suggest that the pyroxene dissolution is initiated by the relatively rapid removal of Mg atoms at edge positions via Mg–H exchange reaction. This can be expressed as (*e.g.* Oelkers & Schott, 2001)

$$>\mathrm{Mg} + 2\mathrm{H}^+ = \mathrm{Mg}^{2+} + 2\,>\mathrm{H} \qquad (13)$$

where >Mg designates an Mg atom in the pyroxene structure. This exchange reaction partially liberates Si–O tetrahedra, which are subsequently released to solution during mineral dissolution. In agreement with transition-state theory, far-from-equilibrium dissolution rates will therefore be proportional to the concentrations of partially detached

Si tetrahedra. The concentrations of the partially detached Si tetrahedra can be estimated from mass action law for reaction (13) which, when combined with Eq. (3), yields (for detail see Oelkers, 2001):

$$r_+ = k_+ \frac{\left(\frac{a^2_{H+}}{a_{Mg^{2+}}}\right)^{n_i}}{1 + K\left(\frac{a^2_{H+}}{a_{Mg^{2+}}}\right)^{n_i}} \qquad (14)$$

where n_i denotes a stoichiometric coefficient, equal to the number of partially detached Si tetrahedra formed by the removal of each Mg, and K designates the equilibrium constant for reaction (6b). When there is still substantial Mg remaining at the pyroxene edge surface, or $K((a_{H+})^2/(a_{Mi^{2+}}))^{n_i} << 1$, Eq. (14) can be reduced to Eq. (4). See Oelkers (2001).

Experiments indicate that the pyroxene dissolution rates at 100 °C are controlled by the detachment of partially liberated silica tetrahedra at mineral surface, as permitted by the exchange at mineral edges of Mg^{2+} (Fe, Ca) for two protons.

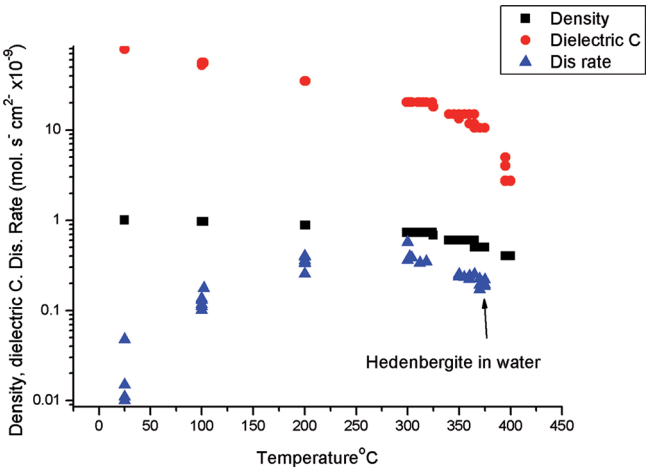

Fig. 10. Dielectric constant and density (g/ml) of water as a function of temperature at 23 MPa; comparison of release rates of Si for pyroxene in water: r_{Si}. 300 °C is an interesting limit for temperature. Below 300 °C, water properties vary slowly. Above 300 °C water properties show strong fluctuations. ■ refers to water dielectric constant, from 2.7 (400 °C) to 78.2 (25 °C); ◆ stands for water density (g/ml) from 0.4 (400 °C to 1 (25 °C) ▲ accounts for release rates of Si of pyroxene (mol $s^{-1}cm^{-2}\times10^{-9}$).

5.2. Effect of the variations of water properties on reaction rates within the critical state region

As mentioned above, dissolution rates (release rate of Si) of pyroxene increase with temperature from 25 to 300 °C and then decrease. The release rates of the other elements show similar trends, reaching a maximal value at various temperatures: at 260 °C for Ca and Al, at 100 °C for Mg and Fe, at 25 °C for Na.

Silica has lower release rates than the other elements at low temperatures, at $T < 300$ °C, higher rates at temperatures ≥300 °C (Fig. 6). The variation of $\Delta m_{Mi}/\Delta m_{Si}$ with temperature is particularly different between the data obtained at $T > 300$ °C and those at $T < 300$ °C. We have already observed this phenomenon in previous silicate dissolution experiments (Zhang *et al.,* 2000, 2002; Zhang *et al.,* 2004): when albite dissolves in water, the release rate of Si increases with temperature from 25 to 300 °C, reaches a maximum at 300 °C, then decreases from 300 °C to 400 °C, and the release ratios ΔNa/ΔSi and ΔAl/ΔSi are higher than the stoichiometric numbers at $T < 300$ °C, and lower than those at $T \geq 300$ °C. The same phenomena were found in experiments on actinolite dissolution in water (Zhang *et al.,* 2004), where the release rate of Si increases with temperature from 25 to 300 °C, reaches a maximum at 300 °C, then decreases. Release rates of most metals (Mg, Fe, Ca, Na, Al) from actinolite are almost higher than release rate of Si at $T < 300$ °C, and lower than the release rate of Si at $T \geq 300$ °C.

This behaviour is related to a change of composition of the leached layer due to variation of temperature. The surface layer is possibly depleted in silica and relatively enriched in other metals at high temperature, whereas at low temperature other metals are preferentially leached out from mineral surface, see Table 5.

Water properties control mineral dissolution processes, and vary strongly at temperatures above 300 °C (Johnson & Norton, 1991; Shaw *et al.,* 1991). Increasing the temperature from 300 °C to 400 °C, at a constant pressure of 23 MPa, induces a strong decrease of the water density, from 0.73 to 0.4 g/ml, and of the dielectric constant, from 20.4 to 2.73. It is conceivable that such strong variations in water properties within the region from a sub-critical to the critical state will affect the dissolution rates of multi-oxide minerals (Fig. 10). Within and near the critical region, the rapid decrease of the dielectric constant and of water density results in the destruction of the hydrogen bond network of the water molecules, which may affect the rates of ionic reactions and the hydration of the silicate framework (Driesner *et al.,* 1998; Zhang & Hu, 2004).

It is generally considered that the Al–O and Si–O bridging bonds exhibit weak ionic and polar (covalent) properties. The Ca–O and Mg–O bridging bonds have relatively ionic bond properties. For pyroxene, certain metal oxygen bonds (*e.g.* Mg–O_{br} Ca–O_{br}) are broken faster than others in water at 25 and 100 °C. As temperature rises (to sub-critical state of water), water density and dielectric constant decrease and the hydrogen bond network of the water molecules is destroyed, thus water becomes gradually capable of dissolving polar-bonded substances (*e.g.* breaking the Si–O bond) whereas breaking the Ca–O, Mg–O, Fe–O bonds becomes increasingly difficult (Jonhson & Norton, 1991; Shaw *et al.,* 1991; Zhang *et al.,* 2002).

Therefore, upon crossing the critical region of water, both the ionic and hydration reactions are weakening. However, owing to differences in polarizability among the different bridging bonds (Ca–O_{br}, Mg–O_{br}, Fe–O_{br}, Al–O_{br} and Si–O_{br}), the Si–O_{br} bond becomes more easily broken and hydrated than at temperatures below 300 °C.

Thus, the release rate of Si is faster than that of other elements at $T \geq 300$ °C, and the leached layer on mineral surface becomes Si-depleted and enriched in other metals.

At temperature above 300 °C, the breaking of octahedral M_i^{2+}–O bonds will occur after the adjoining tetrahedral Si has been removed from the pyroxene structure due to hydration of Si–O–Si. The rates to break octahedral M_i^{2+}–O bonds are slower than those for tetrahedral Si–O bond under the conditions from sub-critical state to the critical state of water. The pyroxene dissolution at temperatures >300 °C is different from that at temperatures <300 °C, as caused by the variation of water properties within the critical region.

Thus, the decrease of dielectric constant and density of water will affect the reactions between water molecules and M_i–O, Si–O–Si bonds, ionic exchange and hydrations at mineral surface, resulting in a dramatic change of the equilibrium constant for the reaction forming the activation complex. These results are depicted in Figs. 9 and 10, and indicate that release rates of Si decrease with increasing temperature at temperature higher than 300 °C.

6. Conclusion

Kinetic experiments demonstrate that pyroxene dissolution rates in pure water vary with temperature in the range from 20 °C to 374 °C, 23 MPa. The experimental results show that Mg dissolves faster than Si at temperatures ≤ 100 °C, Fe and Ca dissolve faster than Si at 25 °C. At temperatures ≥ 200 °C, particularly above 300 °C, Si dissolves faster than the other elements. Maximum release rates of Si in pure water occur at 300 °C.

The experiments indicate that the release ratios, $\Delta m_i/\Delta m_{Si}$ (i = Mg, Ca, Fe) in aqueous solutions vary with temperature. Stoichiometric dissolution of pyroxene in water occurs at 100 °C. Results indicate that pyroxene dissolution rates are pH dependent. As usual, far from equilibrium dissolution rates of pyroxene do not vary strongly with molar concentrations of dissolved Mg, Fe and Ca in the output solution.

The rates in water can be described as Eq. (11):

$$-r_+ = A.\exp(-E_A/RT) \cdot ((a_{H^+})^{Zi}/(a_{Mi})^{Zi+})^{0.165},$$

where $E_A = -22.667$ kJ/mol (pH = 4.8–6.9, from 25 °C to 300 °C), $A = 2.011\ 10^{-7}$ m cm^{-2} s^{-1}. The slope $\alpha = 0.165$ corresponding to log r *vs.* $\log((a_{H^+})^{Zi}/(a_{Mi}{}^{Zi+})^{\alpha}$ and is close to the stoichiometric number of Mg, 0.154.

The dissolution of pyroxene requires the breaking of more than one metal–oxygen bond type. Certain metal–oxygen bonds are broken faster than Si-O_{br} in water at 25 °C and 100 °C. It is likely that some metals (*e.g.* Ca, Mg, Fe,) within the structure can be removed far before the multi-oxide structure is destroyed by dissolution (*e.g.* at $T < 300$ °C). Experiments of pyroxene dissolution in water demonstrate that the hydrolysis of Si–O–Si bond and M_i-H exchange reaction at temperatures < 300 °C are different from the reactions at temperatures ≥ 300 °C and 23 MPa. Because of differences in polarizability among the Ca–O_{br}, Mg–O_{br}, Al–O_{br} and Si–O_{br} bonds, the relatively ionic M_i–O bond more easily breaks than Si–O_{br} at low temperatures (*e.g.* $T = 25$ °C to 100 °C). But the Si–O_{br} bond is faster hydrated at temperatures ≥ 300 °C, as caused by strong variation of water properties: decrease of water density and dielectric constant within the near-critical region. Thus, the rates to break octahedral M_i^{2+} (Ca, Mg, Fe)–O bonds are slower than that to break tetrahedral Si–O bond at temperature above 300 °C.

Acknowledgements: This work was supported by projects of the Ministry of Land and Resources and the Ministry of Science and Technology: k [2013] 01-062-014, SinoProbe-07-02-03, SinoProbe-03-01-2A, 2010G28, and 20010302.

References

Aagaard, P., Helgeson, H.C. (1977): Thermodynamic and kinetic constraints on the dissolution of feldspars. *Geol. Soc. Am.*, **9**, 873 (Abstracts with Program).

—, — (1982): Thermodynamic and kinetic constraints on reaction rates among minerals and aqueous solutions: I. Theoretical considerations. *Am. J. Sci.*, **282**, 237–285.

Alekseyev, V.A., Medvedeva, L.S., Prisyagina, N.I. (1993): Rates of congruent dissolution of feldspars in acid and alkaline hydrothermal solutions. *Geochem. Int.*, **30**, 26–35.

Alekseyev, V.A., Medvedeva, L.S., Prisyagina, N.I., Meshalkin, S.S., Balabin, A.I. (1997): Change in the dissolution rates of alkali feldspars as a result of secondary mineral precipitation and approach to equilibrium. *Geochim. Cosmochim. Acta*, **61**, 1125–1142.

Bauer, A., Berger, G. (1998): Kaolinite and smectite dissolution rate in high molar KOH solutions at 35° and 80 °C. *Appl. Geochem.*, **13**, 905–916.

Brady, P.V., Walther, J.V. (1992): Surface chemistry and silicate dissolution at elevated temperatures. *Am. J. Sci.*, **292**, 639–658.

Brandt, F., Bosbach, D., Krawczyk-Barsch, E., Arnold, T., Bernhard, G. (2003): Chlorite dissolution in the acid pH-range: A combined microscopic and macroscopic approach. *Geochim. Cosmochim. Acta*, **67**, 1451–1461.

Brantley, S.L., Chen, Y. (1995): Chemical weathering rates of pyroxenes and amphiboles. *Rev. Miner. Geochem.*, **31**(1), 119–172.

Cama, J., Ganor, J., Ayora, C., Lasaga, A.C. (2000): Smectite dissolution kinetics at 80° and pH 8.8. *Geochim. Cosmochim. Acta*, **64**, 2701–2717.

Carroll, S.A., Knauss, K.G. (2005): Dependence of labradorite dissolution kinetics on CO_2(aq), Al-(aq), and temperature. *Chem. Geol.*, **217**, 213–225.

Casey, W.H., Hochella, M.F., Jr, Westrich, H.R. (1993): The surface chemistry of manganiferous silicate minerals as inferred from experiments on tephroite (Mn_2SiO_4). *Geochim. Cosmochim. Acta*, **57**, 785–793.

Chaïrat, C., Schott, J., Oelkers, E.H., Lartigue, J.-E., Harouiya, N. (2007): Kinetics and mechanism of natural fluorapatite dissolution at 25 °C and pH from 3 to 12. *Geochim. Cosmochim. Acta*, **71**, 5901–5912.

Chen, Y., Brantley, S.L. (1998): Diopside and anthophyllite dissolution at 25°and 90 °C and acid pH. *Chem. Geol.*, **147**, 233–248.

Chou, L., Wollast, R. (1984): Study of the weathering of albite at room temperature and pressure with a fluidized bed reactor. *Geochim. Cosmochim. Acta*, **48**, 2205–2218.

Devidal, J.L., Schott, J., Dandur, J.L. (1997): An experimental study of kaolinite dissolution and precipitation kinetics as a function of chemical affinity and solution composition at 150 °C, 40 bars, and pH 2, 6.8, and 7.8. *Geochim. Cosmochim. Acta*, **61**, 5165–5186.

Dixit, S., Carroll, S.A. (2007): Effect of solution saturation state and temperature on diopside dissolution. *Geochem. Trans.*, **8**, 3 http://www.geochemicaltransactions.com/content/8/1/3.

Dove, P.M. (1999): The dissolution kinetics of quartz in aqueous mixed cation solutions. *Geochim. Cosmochim. Acta*, **63**, 3715–3727.

Dove, P.M., Crerar, D.A. (1990): Kinetics of quartz dissolution in electrolyte solutions using a hydrothermal mixed flow rector. *Geochim. Cosmochim. Acta*, **54**, 955–969.

Driesner, T., Seward, T.M., Tironi, J.G. (1998): Molecular dynamics simulation study of ionic hydration and ion association in dilute and 1 molal aqueous sodium chloride solution from ambient to supercritical conditions. *Geochim. Cosmochim. Acta*, **62**, 3095–3107.

Frogner, P., Schweda, P. (1998): Hornblende dissolution kinetics at 25 °C. *Chem. Geol.*, **151**, 169–179.

Gautier, J.-M., Oelkers, E.H., Schott, J. (1994): Experimental study of K-feldspar dissolution rates as a function of chemical affinity at 150 °C and pH 9. *Geochim. Cosmochim. Acta*, **58**, 4549–4560.

Guy, B. (2003): Use of chemical potential phase diagrams to discuss aqueous saturation and precipitation/dissolution kinetics of solid solutions. Abstract volume of the international conference, Gas-water rock interactions induced by reservoir exploitation, CO_2 sequestration, and other geological storage held at I.F.P., Rueil-Malmaison, France (18–20 November).

Harouiya, N., Oelkers, E.H. (2004): An experimental study of the effect of aqueous fluoride on quartz and alkali-feldspar dissolution rates. *Chem. Geol.*, **205**(1–2), 155–167.

Helgeson, H.C., Murphy, W.M., Aagaard, P. (1984): Thermodynamic and kinetic constraints on reaction rates among minerals and aqueous solutions: II. Rate constants, effective surface area, and the hydrolysis of feldspar. *Geochim. Cosmochim. Acta*, **48**, 2405–2432.

Hellmann, R., Crerar, D., Zhang, R.H.. (1989): Albite feldspar hydrolysis to 300 °C. *Solid State Ionics*. **32/33**, In reactivity of solids., Proc. 11th S., 314–329.

Hofmann, H., Bauer, A., Warr, L.N. (2004): Behavior of smectite in strong salt brines under conditions relevant to the disposal of lowtomedium-grade nuclear waste. *Clays Clay Minerals*, **52**, 14–24.

Jiana, C.J., (1993): Etude des alternances récurrentes dans les skarns et des instabilités du front de dissolution/précipitation, PhD thesis, Ecole Nationale Supérieure des Mines de Saint-Etienne, 196.

Jonhson, J.W., Norton, D. (1991): Critical phenomena in hydrothermal systems: state, thermodynamic, electrostatic, and transport properties of H_2O in the critical region. *Am. J. Sci.*, **291**, 541–648.

Johnson, J.W., Oelkers, E.H., Helgeson, H.C. (1992): SUPCRT 92–a software package for calculating the standard molal thermodynamic properties of minerals, gases, aqueous species, and reactions from 1-bar to 5000-bar and 0 °C to 1000 °C. *Comput. & Geosci.*, **18**(7), 899–947.

Knauss, K.G., Wolery, T.J. (1986): Dependence of albite dissolution kinetics on pH and time at 70 °C. *Geochim. Cosmochim. Acta*, **50**, 2481–2497.

—, — (1989): Muscovite dissolution kinetics as a function of pH and time at 70 °C. *Geochim. Cosmochim. Acta*, **53**, 1493–1502.

Knauss, K.G., Nguyen, S.N., Weed, H.C. (1993): Diopside dissolution kinetics as a function of pH, CO_2, temperature, and time. *Geochim. Cosmochim. Acta*, **57**, 285–294.

Kohler, S., Dufaud, F., Oelkers, E.H. (2003): An experimental study of illite dissolution rates as a function of pH from 1.4 to 12.4 and temperature from 5 to 50 °C. *Geochim. Cosmochim. Acta*, **67**, 3583–3594.

Lasaga, A.C. (1981): Rate laws of chemical reactions. *in* ''Kinetics of geochemical processes'', A.C. Lasaga & R.J. Kirkpatrick (eds.), *Rev. Mineral*., **8**, 1–68.

Levelt Sengers, J.M.H. (2000): Supercritical fluids, fundamentals and applications, NATO Advanced Science Institute, Series E: Applied Sciences, Vol. 366, Ch. 1, pp. 1–29. E. Kiran, P.G. Debenedetti, C.J. Peters (eds.) Kluwer Academic Publishers, Dordrecht, Netherlands.

Metz, V., Amram, K., Ganor, J. (2005): Stoichiometry of smectite dissolution reaction, *Geochim. Cosmochim. Acta*, **69**(7), 1755–1772.

Murphy, W.M., Helgeson, H.C. (1987): Thermodynamic and kinetic constraints on reaction rates among minerals and aqueous solutions. lll. Activated complexes and the pH-dependence of the rates of feldspar, pyroxene, and olivine hydrolysis. *Geochim. Cosmochim. Acta*, **51**, 3137–3153.

—, — (1989): Thermodynamic and kinetic constraints on reaction rates among minerals and aqueous solutions. lV. Retrieval of rate constants and activation parameters for the hydrolysis of pyroxene, wollastonite, olivine andalusite, quartz, and nepheline. *Am. J. Sci.*, **289**, 17–101.

Nagy, K.L. (1995): Dissolution and precipitation kinetics of sheet silicates. *in* ''Chemical Weathering Rates of Silicate Minerals'', A.F. White & S.L. Brantley, eds. Mineralogical Society of America, Washington, DC, Vol. 31, 173–233.

Nagy, K.L., Lasaga, A.C. (1992): Dissolution and precipitation kinetics of gibbsite at 80 °C and pH 3–The dependence on solution saturation state. *Geochim. Cosmochim. Acta*, **56**(8), 3093–3111.

Nourtier-Mazauric, E., Guy, B., Fritz, B., Brosse, E., Garcia, D., Clément, A. (2005): Modeling the Dissolution/Precipitation of Ideal Solid Solutions. *Oil & Gas Science and Technology Rev. IFP.*, **60**(2), 401–415.

Oelkers, E.H. (2001): An experimental study of forsterite dissolution rates as a function of temperature and aqueous Mg and Si concentrations. *Chem. Geol.*, **175**, 485–494.

Oelkers, E.H., Schott, J. (1999): Experimental study of kyanite dissolution rates as function of chemical affinity and solution composition. *Geochim. Cosmochim. Acta*, **63**, 785–797.

—, — (2001): An experimental study of enstatite dissolution rates as a function of pH, temperature, and aqueous Mg and Si concentration, and the mechanism of pyroxene/pyroxenoid dissolution. *Geochim.Cosmochim. Acta*, **65**(8), 1219–1231.

Oelkers, E.H., Schott, J., Devidal, J.L. (1994): The effect of aluminum, pH, and chemical affinity on the rates of aluminosilicate dissolution reactions. *Geochim. Cosmochim. Acta*, **58**(201), 1–2024.

Oelkers, E.H., Schott, J., Gauthier, J.-M., Herrero-Roncal, T. (2008): An experimental study of the dissolution mechanism and rates of muscovite. *Geochim. Cosmochim. Acta*, **72**(20), 4948–4961.

Peck, J.A., Farnan, I., Stebbins, J.F. (1988): Disordering and the progress of hydration at the surface of diopside; a crosspolarisation MAS NMR study. *Geochim. Cosmochim. Acta*, **52**, 3017–3021.

Petit, J.C., Della, M.G., Dran, J.C., Schott, J., Berner, R.A. (1987): Mechanism of diopside dissolution from hydrogen depth profiling. *Nature*., **325**, 705–707.

Petrović, R. (1976): Rate control in feldspar dissolution – II. The protective effect of precipitates. *Geochim. Cosmochim. Acta*, **40**, 1509–1521.

Petrovich, J.D. (1981): Kinetics of dissolution of mechanically comminuted rock – forming oxides and silicates: l. Deformation and dissolution of quartz under laboratory conditions. *Geochim. Cosmochim. Acta*, **45**, 1667–1674.

Pokrovsky, O.S., Schott, J. (2000): Kinetics and mechanism of forsterite dissolution at 25 °C and pH from 1 to 12. *Geochim. Cosmochim. Acta*, **64**(19), 3313–3325.

Saldi, G.D., Köhler, S.J., Marty, N., Oelkers, E.H. (2007): Dissolution rates of talc as a function of solution composition, pH and temperature. *Geochim. Cosmochim. Acta*, **71**, 3446–3457.

Sato, T., Kuroda, M., Yokoyama, S., Fukushi, K., Tanaka, T., Nakayama, S. (2003): Mechanism and kinetics of smectite dissolution under alkaline conditions. *Geochim. Cosmochim. Acta*, **67**(18), A415.

Schott, J., Berner, R.A. (1985): Dissolution mechanisms of pyroxenes and olivines during weathering. In: The chemistry of weathering, vol. 149, J. I. Drever, ed., *NATO ASI* series C; Mathematical and Physical Sciences, 35–53.

Schott, J., Petit, J.C. (1987): New evidence for the mechanisms of dissolution of silicate minerals. *in* ''Aquatic surface chemistry: chemical processes at the mineral-surface interface'', W. Stumm, ed. Swiss Federal Institute of Technology Zurich, Switzerland, 293–315.

Schott, J., Berner, R.A., Sjoberg, E.L. (1981): Mechanism of pyroxene and amphibole weathering—I. Experimental studies of iron-free minerals. *Geochim. Cosmochim. Acta*, **45**, 2123–2135.

Schott, J., Pokrovsky, O.S., Oelkers, E. (2009): The link between mineral dissolution/precipitation kinetics and solution chemistry. *Reviews in Mineralogy & Geochemistry.*, **70**, 207–258.

Shaw, R.W., Brill, T.B., Ecker, C.A., Frank, E.U. (1991): Supercritical water, Special Report. *C&EN*, **23**, 26–39.

Shvarov, Yu.W. (1989): A numerical criterion for existence of the equilibrium state in an open chemical system. *Sci. Geol., Bull.*, **42**, 365–369.

Stillings, L.L., Brantley, S.L. (1995): Feldspar dissolution at 25 °C and pH 3: Reaction stoichiometry and the effect of cations. *Geochim. Cosmochim. Acta*, **59**, 1483–1496.

Stillings, L.L., Brantley, S.L., Machesky, M.L. (1995): Proton adsorption at an adularia feldspar surface. *Geochim. Cosmochim. Acta*, **59**, 1473–1482.

Stillings, L.L., Drever, J.I., Brantley, S.L., Sun, Y., Oxburgh, R. (1996): Rates of feldspar dissolution at pH 3–7 with 0–8 mM oxalic acid. *Chem. Geol.*, **132**, 79–89.

Sutheimer, S.H., Maurice, P.A., Zhou, Q. (1999): Dissolution of well and poorly crystallized kaolinites: Al speciation and effects of surface characteristics. *Am. Mineral*, **84**, 620–628.

Welch, S.A., Ullman, W.J. (1993): The effect of organic acids on plagioclase dissolution rates and stoichiometry. *Geochim. Cosmochim. Acta*, **57**, 2725–2736.

—, — (1996): Feldspar dissolution in acidic and organic solutions: Compositional and pH dependence of dissolution rate. *Geochim. Cosmochim. Acta*, **60**, 2939–2948.

Wieland, E., Wehrl, B., Stumm, W. (1988): The coordination chemistry of weathering: III. A generalization on the dissolution of minerals. *Geochim. Cosmochim. Acta*, **52**, 1969–1981.

Zhang, R.H., Hu, S.M. (2004): Hydrothermal study using a new diamond anvil cell with in situ IR spectroscopy under high temperatures and high pressures. *J. Supercritical Fluids*, **29**, 185–202.

Zhang, R.H., Posey-Dowty, J., Hellmann, R., Borcsik, M., Crerar, D., Hu, S. (1990): Kinetics of mineral-water reactions in hydrothermal flow systems at elevated temperatures and pressures. *Science in China (Series B)*, **33**(9), 1136–1152 (English edition).

Zhang, R.H., Hu, S., Zhang, X.T. (2000): Kinetics of hydrothermal reactions of minerals in near-critical and supercritical water. *Acta Geol. Sinica*, **74**, 400–405.

Zhang, R., Hu, S., Su, Y. (2002): Alteration zoning and kinetic process of mineral – water interactions, *Acta Geol. Sinica*, **76**(3), 351–366.

Zhang, R., Hu, S., Zhang, X. (2004): Kinetics study of silicate mineral dissolution in water at high temperatures near to the critical point of water. *in* ''Water–Rock interaction'', R.B. Wanty & R.R. Seal II, eds. Taylor & Francis Group, London, 321–324.

—, (2006): Experimental study of dissolution rates of fluorite in HCl-H_2O Solution. *Aquatic Geochem.*, **12**, 123–159.

Zhang, R.H., Zhang, X.T., Hu, S.M., Su, Y.F. (2007a): Kinetic experiments of water rock interactions at high temperatures and high pressures corresponding to the middle crust conditions. *Acta Petrologica Sinica*, **23**(11), 2933–2942.

Zhang, R.H., Zhang, X.T., Hu, S.M. (2007b): Experimental study of dissolution rates of multi-oxide silicates in water up to 400°C, Proceedings of the 12th International Symposium on Water-Rock Interaction WRI-12, Water- rock interaction, Bullen & Wang (eds), Taylor & Francis Group, London, 2007, 1, 403–406.

Zhu, C., Veblen, D.R., Blum, A.B., Chipera, S.J. (2006): Naturally weathered feldspar surfaces in the Navajo Sandstone aquifer, Black Mesa, Arizona: Electron microscopic characterization. *Geochim. Cosmochim. Acta*, **70**, 4600–4616.

Zhu, C., Lu, P., Zheng, Z., Ganor, J. (2010): Coupled alkali feldspar dissolution and secondary mineral precipitation in batch systems: 4. Numerical modeling of kinetic reaction paths. *Geochim. Cosmochim. Acta*, **74**, 3963–3983.

Received 19 June 2012
Modified version received 12 February 2013
Accepted 14 February 2013

Appendix 1. Steady state dissolutions and stoichiometry

Previous studies suggest that steady-state dissolution is defined as a constant concentration of dissolved metals in the output solution over time. When the system eventually reaches steady state, constant concentrations of the aqueous species and constant reaction rates are expected (Cama *et al.,* 2000; Dixit & Carroll, 2007). Some investigators suggest that steady-state kinetics is defined when dissolution rates are time independent and dissolution is stoichiometric (*e.g.,* Oelkers & Schott, 2001). These studies do not discuss incongruent dissolution.

Our reactor was heated to the desired temperature and pressure and the input solution was driven through the reactor at a constant flow rate until the outlet solution attained a steady state concentration (*e.g.,* Ca, Mg and Si). Steady state outlet concentrations were obtained after an elapsed time ranging from 2 hours to 2 days, depending on the flow rate and stirred rates (using stirred flow reactor). Thus, this study defined steady state: the concentrations of dissolved metals in output solutions did not change with elapsed time.

Reaction stoichiometry was examined by comparing release ratios of molar concentrations of $\Delta m_i/\Delta m_{Si}$ in the effluent solution with the stoichiometric numbers of moles of these elements in the pyroxene. Δm_i stands for the difference between the inlet and outlet fluid concentration of the subscripted metal i, such as Mg, Ca, Fe etc. $\Delta m_i = m_{i\ (outlet)} - m_{i,\ 0\ (inlet)}$

When dissolution is stoichiometric, $\Delta m_i/\Delta m_{Si}$ in the effluent solution (or r_{Mi}/r_{Si}) is the same as the stoichiometric number of moles of these elements in the mineral, N_i. Experiments for pyroxene in water indicate that the release rates for each metal, *e.g.,* Ca, Mg, Al, Na, and Si, vary with temperature (Fig. 2). Simultaneously, molar concentration ratios $\Delta m_i/\Delta m_{Si}$ for Ca/Si, Mg/Si, Fe/Si, Al/Si in solutions vary with temperature (Fig. 3). In most cases, $\Delta m_i/\Delta m_{Si}$ ratios for M*i*/Si in solutions are different from the stoichiometric number of moles of these elements in the solid, Ni.

We waited sufficient time for pyroxene-water reaction to reach a steady state at a fixed condition; then concentrations of most Mi are constant. At that time, ratios $\Delta m_i/\Delta m_{Si}$ are constant. We changed flow rates (0.8ml/min to 3.6 ml/min) in a long period of time. Results indicate that molar concentration ratios $\Delta m_i/\Delta m_{Si}$ for Ca/Si, Mg/Si, Fe/Si, Al/Si in solution are almost constant with varying flow rates, and the experiments were performed during more than 2 days. See Fig. 4. The $\Delta m_i/\Delta m_{Si}$ ratios are time independent. We can measure the steady state release rates for each dissolved metal at different temperatures. But the steady state dissolution rates at 25 °C, 200 °C, 300 °C, 374 °C are not stoichiometric. Pyroxene dissolution is near stoichiometric only at 100 °C (Fig. 3). Previous studies reported steady state dissolution rates for albite in water at temperatures from 20 to 400 °C, but albite dissolution is stoichiometric only at 300 °C (see Hellmann *et al.,* 1989; Zhang *et al.,* 2002).

Appendix 2

Based on the composition of the measured molar concentrations of dissolved metals in the effluent solutions, one can assess the speciation of the dissolved metals in the solution under experimental conditions by using HCh (Shvarov, 1989).

Table A. Calculation example for speciation of effluent solution based on measured composition of the effluent fluids as pyroxene reacted with HCl-H_2O at pH 3.85 to 4.6.

H_2O	0	9.999383E-01*	1.00000*	9.999400E-01*	1.00000*	9.999581E-01*	1.00000*
H^+	1	1.408538E-04	0.92215	1.346840E-04	0.92322	5.849378E-05	0.93757
OH^-	2	7.757544E-08	0.91598	8.092524E-08	0.91723	1.802555E-07	0.93366
$H_3SiO_4^-$	3	1.118603E-08	0.91718	1.141016E-08	0.91839	1.820306E-08	0.93441
H_4SiO_4	4	9.083410E-04	0.99994	8.881531E-04	0.99994	6.358204E-04	0.99996
O_2	5	3.739384E-04	0.99994	4.491034E-04	0.99994	4.306798E-04	0.99996
H_2	6	1.199229E-22	0.99994	1.094281E-22	0.99994	1.117431E-22	0.99996
Cl^-	7	1.273117E-03	0.91537	1.223834E-03	0.91664	7.707642E-04	0.93328
HCl	8	3.727548E-06	0.99994	3.434997E-06	0.99994	9.714593E-07	0.99996
Na^+	9	6.046304E-05	0.91658	5.038856E-05	0.91781	3.024845E-05	0.93404
NaOH	10	8.291278E-11	0.99994	7.227592E-11	0.99994	1.001119E-10	0.99996
NaCl	11	9.369275E-08	0.99994	7.526295E-08	0.99994	2.948299E-08	0.99996
K^+	12	3.016948E-05	0.91537	3.017332E-05	0.91664	1.006978E-04	0.93328
KOH	13	1.974027E-11	0.99994	2.065172E-11	0.99994	1.591034E-10	0.99996
KCl	14	1.089061E-07	0.99994	1.049926E-07	0.99994	2.287600E-07	0.99996
Mg^{2+}	15	9.420640E-05	0.71969	8.761657E-05	0.72313	3.184988E-05	0.77040
$MgOH^+$	16	3.373851E-08	0.91718	3.289147E-08	0.91839	2.838642E-08	0.93441
$MgCl^+$	17	4.669305E-06	0.91718	4.194815E-06	0.91839	1.023855E-06	0.93441
$MgCl_2$	18	1.174307E-11	0.99994	1.016873E-11	0.99994	1.619243E-12	0.99996

Table A. Continued.

Ca_2^+	19	4.067431E-04	0.71285	4.051023E-04	0.71647	2.561808E-04	0.76582
$CaOH^+$	20	8.404196E-08	0.91718	8.776340E-08	0.91839	1.322008E-07	0.93441
$CaCl^+$	21	9.849411E-06	0.91718	9.478304E-06	0.91839	4.037845E-06	0.93441
$CaCl_2$	22	1.561776E-07	0.99994	1.448651E-07	0.99994	4.026264E-08	0.99996
Fe_{++}	23	2.826459E-10	0.71285	9.661216E-11	0.71647	1.037220E-12	0.76582
$FeOH^+$	24	1.207558E-11	0.91718	4.327829E-12	0.91839	1.106746E-13	0.93441
$Fe(OH)_2$	25	2.707272E-14	0.99994	1.014882E-14	0.99994	5.987071E-16	0.99996
$Fe(OH)_3^-$	26	1.453219E-19	0.91718	5.683191E-20	0.91839	7.471451E-21	0.93441
$FeCl^+$	27	6.284546E-12	0.91718	2.075578E-12	0.91839	1.501119E-14	0.93441
$FeCl_2$	28	6.069098E-15	0.99994	1.932030E-15	0.99994	9.116110E-18	0.99996
Fe^{3+}	29	1.203433E-14	0.45905	4.094322E-15	0.46454	1.754659E-17	0.54290
$FeOH^{2+}$	30	3.468345E-09	0.70751	1.240796E-09	0.71125	1.314763E-11	0.76227
$Fe(OH)_2^+$	31	2.517858E-05	0.91718	9.446705E-06	0.91839	2.390650E-07	0.93441
$Fe(OH)_3$	32	9.088315E-05	0.99994	3.566597E-05	0.99994	2.082145E-06	0.99996
$Fe(OH)_4^-$	33	1.720338E-09	0.91718	7.043071E-10	0.91839	9.162895E-11	0.93441
$FeCl^{2+}$	34	7.550655E-14	0.70751	2.489236E-14	0.71125	7.459527E-17	0.76227
		I	0.002	I	0.002	I	0.001
		pH	3.886	pH	3.905	pH	4.261
		Eh	0.609	Eh	0.609	Eh	0.571